



Deposited via The University of York.

White Rose Research Online URL for this paper:

<https://eprints.whiterose.ac.uk/id/eprint/173866/>

Version: Accepted Version

Article:

Chan, Yuk-Chun, Evans, Mathew J., He, Pengzhen et al. (2021) Heterogeneous Nitrate Production Mechanisms in Intense Haze Events in the North China Plain. *Journal of Geophysical Research: Atmospheres*. e2021JD034688. ISSN: 2169-8996

<https://doi.org/10.1029/2021JD034688>

Reuse

Items deposited in White Rose Research Online are protected by copyright, with all rights reserved unless indicated otherwise. They may be downloaded and/or printed for private study, or other acts as permitted by national copyright laws. The publisher or other rights holders may allow further reproduction and re-use of the full text version. This is indicated by the licence information on the White Rose Research Online record for the item.

Takedown

If you consider content in White Rose Research Online to be in breach of UK law, please notify us by emailing eprints@whiterose.ac.uk including the URL of the record and the reason for the withdrawal request.

Heterogeneous nitrate production mechanisms in intense haze events in the North China Plain

Yuk-Chun Chan¹, Mathew J. Evans^{2,3}, Pengzhen He⁴, Christopher D. Holmes⁵, Lyatt Jaeglé¹, Prasad Kasibhatla⁶, Xue-Yan Liu⁷, Tomás Sherwen^{2,3}, Joel A. Thornton¹, Xuan Wang⁸, Zhouqing Xie⁹, Shuting Zhai¹, and Becky Alexander¹

¹Department of Atmospheric Sciences, University of Washington, Seattle, WA 98195, USA

²National Centre for Atmospheric Science, University of York, York, YO10 5DD, UK

³Wolfson Atmospheric Chemistry Laboratories, Department of Chemistry, University of York, York, YO10 5DD, UK

⁴School of Environment and Tourism, West Anhui University, Lu'an, Anhui 237012, China

⁵Department of Earth, Ocean and Atmospheric Science, Florida State University, Tallahassee, FL 32306, USA

⁶Nicholas School of the Environment, Duke University, Durham, NC 27708, USA

⁷School of Earth System Science, Tianjin University, Tianjin, China

⁸School of Energy and Environment, City University of Hong Kong, Hong Kong SAR, China

⁹Anhui Key Laboratory of Polar Environment and Global Change, Department of Environmental Science and Engineering, University of Science and Technology of China, Hefei, Anhui, 230026, China

Corresponding author: Becky Alexander (beckya@uw.edu)

Key Points:

- Wintertime observations of ¹⁷O excess of nitrate in Beijing suggest that the heterogeneous chemistry of NO₂ is a weak source of nitrate in intense haze.
- Ozone strongly modulates nitrate production during intense wintertime haze events in Beijing via the heterogeneous chemistry of N₂O₅.

29 **Abstract**

30 Studies of wintertime air quality in the North China Plain (NCP) show that particulate-nitrate
31 pollution persists despite rapid reduction in NO_x emissions. This intriguing NO_x -nitrate
32 relationship may originate from non-linear nitrate-formation chemistry, but it is unclear which
33 feedback mechanisms dominate in NCP. In this study, we re-interpret the wintertime
34 observations of ^{17}O excess of nitrate ($\Delta^{17}\text{O}(\text{NO}_3^-)$) in Beijing using the GEOS-Chem (GC)
35 chemical transport model to estimate the importance of various nitrate-production pathways and
36 how their contributions change with the intensity of haze events. We also analyze the
37 relationships between other metrics of NO_y chemistry and $[\text{PM}_{2.5}]$ in observations and model
38 simulations. We find that the model on average has a negative bias of -0.9‰ and -36% for
39 $\Delta^{17}\text{O}(\text{NO}_3^-)$ and $[\text{O}_{x,\text{major}}](\equiv [\text{O}_3] + [\text{NO}_2] + [\text{p-NO}_3^-])$, respectively, while overestimating the
40 nitrogen oxidation ratio ($[\text{NO}_3^-]/([\text{NO}_3^-] + [\text{NO}_2])$) by $+0.12$ in intense haze. The discrepancies
41 become larger in more intense haze. We attribute the model biases to an overestimate of NO_2 -
42 uptake on aerosols and an underestimate in wintertime O_3 concentrations. Our findings highlight
43 a need to address uncertainties related to heterogeneous chemistry of NO_2 in air-quality models.
44 The combined assessment of observations and model results suggest that N_2O_5 uptake in aerosols
45 and clouds is the dominant nitrate-production pathway in wintertime Beijing, but its rate is
46 limited by ozone under high- NO_x -high- $\text{PM}_{2.5}$ conditions. Nitrate production rates may continue
47 to increase as long as $[\text{O}_3]$ increases despite reduction in $[\text{NO}_x]$, creating a negative feedback that
48 reduces the effectiveness of air pollution mitigation.

49

50 **Plain Language Summary**

51 Nitrate, a major component of particles in urban air, has been identified as an important driver
52 for recent trends in wintertime haze in the North China Plain. While it has long been known that
53 many chemical reactions can convert gas-phase nitrogen oxides into particulate nitrate in the
54 atmosphere, the contribution from different reactions in intense haze remains elusive. Recently,
55 analysis of oxygen stable isotopes (^{16}O , ^{17}O , ^{18}O) in nitrate has become a promising tool for
56 understanding its chemical origins. In this study, we re-examine the isotopic observations of
57 nitrate in wintertime Beijing and compare them with predictions made by an air-quality model.
58 Our analysis of observations suggests that the model likely overestimates nitrate production via
59 the reactions between nitrogen dioxide gas (NO_2) and particles during intense haze events. After
60 removing this nitrate formation pathway in the model, we demonstrate that nitrate production
61 during intense haze events in Beijing is strongly modulated by ozone, a secondary pollutant
62 whose formation is dependent on nitrogen oxides and volatile organic compounds (VOCs).
63 Policies that result in a reduction of ozone concentrations, possibly through reductions in VOC
64 emissions, will also reduce the formation of nitrate during wintertime haze events.

65 1 Introduction

66

67 Haze events, which are episodes of high concentrations of particulate matter (PM) in the lower
68 troposphere, are common in many metropolitan areas around the world. Industrial activities,
69 heavy traffic, and weak ventilation all favor the occurrence of haze events near population
70 centers. The North China Plain, in particular, has been affected by intense wintertime haze in
71 recent decades (An et al., 2019; Y.-L. Zhang & Cao, 2015). Frequent outbreaks of haze events
72 can lead to short-term surges in premature mortality and long-term reduction in life expectancy
73 (Y. Chen et al., 2013; Lelieveld et al., 2015; C. Song et al., 2017). An important source of fine-
74 mode PM (PM_{2.5}, particulate matter with an aerodynamic diameter of equal to or less than 2.5
75 μm) during haze events is chemical reactions that oxidize gas-phase pollutants into PM_{2.5}. To
76 mitigate haze events in metropolitan areas effectively, we must understand the chemical
77 mechanisms driving this secondary production of PM_{2.5}.

78

79 Nitrate is becoming the dominant inorganic component of PM_{2.5} over China in recent years,
80 especially during wintertime haze events (Fu et al., 2020; Itahashi et al., 2018; H. Li et al., 2019;
81 Y. Sun et al., 2020; Xu et al., 2019; Zhou et al., 2019). The Chinese government implemented a
82 series of clean air policies since the year 2010 that imposed stricter controls on the emissions of
83 SO₂, NO_x (NO+NO₂), and primary PM (Zheng et al., 2018). As a result, wintertime sulfate
84 concentration decreased substantially by about 60% from 2014 to 2017 (H. Li et al., 2019; Zhou
85 et al., 2019). A similar long-term concentration reduction was not observed in particulate nitrate
86 (p-NO₃⁻) despite a steady decline in NO_x emission in the 2010s (Fu et al., 2020; Itahashi et al.,
87 2018; H. Li et al., 2019; Xu et al., 2019). Analysis of the aerosol sampled in Beijing in 2017
88 showed that nitrate contributes 25-35% to fine-mode-PM mass during wintertime haze events
89 (H. Li et al., 2019; Xu et al., 2019), which is higher than similar observations in 2014 (<20%)
90 (H. Li et al., 2019). In the eastern US and northern China, the concentration of wintertime
91 secondary aerosol, including nitrate and sulfate, also responds weakly to the reduction of NO_x
92 and SO₂ emissions, which is largely attributed to non-linear chemical feedbacks (Huang et al.,
93 2021; Le et al., 2020; Leung et al., 2020; Shah et al., 2018; Y. Sun et al., 2020). In light of the
94 emerging importance of nitrate in PM pollution in the North China Plain, it is essential to
95 understand the chemistry of nitrate production during wintertime haze events in order to
96 implement effective air pollution mitigation strategies.

97

98 Reactions of reactive nitrogen oxides (NO_y \equiv NO_x + NO₃ + 2×dinitrogen pentoxide (N₂O₅) +
99 nitryl chloride (ClNO₂) + gas-phase nitric acid (HNO₃) + particulate nitrate (p-NO₃⁻) + nitrous
100 acid (HONO) + halogen nitrates (ξNO_3 , where $\xi = \text{Br, Cl, or I}$) + peroxyxynitric acid (HNO₄) +
101 peroxyacylnitrates (PANs) + other organic nitrates (RONO₂)) control both nitrate production and
102 oxidant budgets in the North China Plain (See Figure 1 and Table S1). Production of NO₃⁻ (total
103 nitrate NO₃⁻ = HNO₃ + p-NO₃⁻) is the main sink of NO_x in polluted urban air (Kenagy et al.,
104 2018; Shah et al., 2020). In Beijing, the majority of locally produced HNO₃ quickly converts into
105 p-NO₃⁻ via thermodynamically controlled gas-particle partitioning (Ding et al., 2019). The
106 dominant chemical pathway for nitrate production varies diurnally and seasonally. During the
107 daytime, the oxidation of NO₂ by hydroxyl radical (OH) (Figure 1b, R4) dominates nitrate
108 production, whereas the reactions of nitrate radical (NO₃) (Figure 1b, R8-12), including N₂O₅
109 uptake (Figure 1b, R10-11), dominate at night (Alexander et al., 2020). Shah et al. (2020)
110 showed that N₂O₅ uptake and OH oxidation contribute similarly to NO_x loss (33% vs. 43% in

111 2017) over summertime in central-eastern China, which is similar to the global annual average
112 (41-42% vs. 28-41%) (Alexander et al., 2020). In winter, on the contrary, N_2O_5 uptake dominates
113 over OH oxidation (51% vs. 23%) (Shah et al., 2020). The conversion of NO_x to NO_3^- is coupled
114 to many other reactive species in the atmosphere, including ozone, peroxy radicals (RO_2), and
115 HONO. For instance, the production of NO_3 radical requires ozone (Figure 1b, R6); yet the
116 efficiency of ozone production is, in turn, controlled by the amount of NO_x and peroxy radicals.
117 Meanwhile, the uptake of NO_2 on aerosols (Figure 1b, R5) and photolysis of p-NO_3^- can produce
118 HONO, which yields OH readily upon photolysis and may control the tropospheric oxidizing
119 capacity during haze events (L. Li et al., 2018; Z. Tan et al., 2019; J. Zhang et al., 2019). A
120 comprehensive representation of nitrate chemistry in models is necessary for accurate predictions
121 of air quality in winter.

122
123 While heterogeneous chemistry (i.e., multi-phase reactions) of NO_y is critical to wintertime
124 nitrate production in urban air, its complexity represents a major source of uncertainty in many
125 air-quality models. The uptake of NO_2 on aerosols, which has been presumed to be a sink of NO_x
126 and a source of NO_3^- and HONO in models, was re-examined in recent modeling studies.
127 Holmes et al. (2019) decreased the uptake coefficients of NO_2 ($\gamma(\text{NO}_2)$) in their model after
128 considering the lower estimates of $\gamma(\text{NO}_2)$ reported in more recent laboratory studies. Jaeglé et
129 al. (2018) showed that changing the HONO yield of NO_2 uptake to 100% (no HNO_3 formation)
130 improves the simulation of NO_y chemistry over wintertime Northeast United States. A global
131 model study by Alexander et al. (2020) demonstrated that NO_2 uptake has the largest potential
132 influence over the North China Plain. For N_2O_5 uptake on aerosol, the efficiency of nitrate
133 formation is sensitive to the chemical composition (e.g., $[\text{Cl}^-]$, $[\text{p-NO}_3^-]$, and thickness of
134 organic coating), pH, and water content of aerosols (Bertram & Thornton, 2009; Gaston et al.,
135 2014; Tham et al., 2016; Xia et al., 2019; Zhou et al., 2018). Laboratory-based predictions of the
136 uptake coefficient of N_2O_5 ($\gamma(\text{N}_2\text{O}_5)$) on aerosols often differ from the observation-based
137 estimates by orders of magnitudes (e.g., McDuffie et al., 2018; C. Yu et al., 2020). In addition to
138 reactions on aerosol surfaces, recent modeling studies also suggest that uptake of NO_y in cloud
139 droplets is an overlooked sink of NO_x (Holmes et al., 2019). Cloud uptake of NO_y contributes up
140 to 25% NO_x loss at higher latitudes annually (Alexander et al., 2020; Holmes et al., 2019). Given
141 the large number of remaining uncertainties in heterogeneous chemistry of NO_y , models need
142 additional observational constraints for improving the representation of these chemical processes
143 in air quality models.

144
145 The oxygen isotopic composition of nitrate provides an independent piece of information related
146 to the formation of nitrate. In particular, ^{17}O excess ($\Delta^{17}\text{O}$) in nitrate, which is determined solely
147 by the relative importance of ozone to other oxidants during the oxidation of the members of
148 NO_y family (Michalski et al., 2003), has proven to be a promising proxy for quantifying nitrate-
149 production mechanisms in various environmental contexts (e.g., Alexander et al., 2020; Geng et
150 al., 2017; Savarino et al., 2013). Shao et al. (2019) analyzed observations of $\Delta^{17}\text{O}(\text{SO}_4^{2-})$ in
151 wintertime Beijing and demonstrated the importance of heterogeneous chemistry for sulfate
152 formation during haze events. For $\Delta^{17}\text{O}(\text{NO}_3^-)$, three previous studies have reported observations
153 in the North China Plain during winter haze events (He et al., 2018; W. Song et al., 2020; Y.
154 Wang et al., 2019). Their analyses of the observations suggested that uptake of N_2O_5 and the
155 oxidation of volatile organic compounds (VOCs) by NO_3 radicals (Figure 1b, R12) dominate
156 wintertime nitrate production near Beijing. However, their interpretation of the observations

157 relies on highly simplified models of nitrate production and several assumptions about the
 158 concentration of radicals in urban air. In this study, we use a 3-D chemical transport model with
 159 coupled HO_x-NO_x-VOC-ozone-halogen-aerosol tropospheric chemistry to re-interpret the
 160 observations of Δ¹⁷O(NO₃⁻) in the North China Plain in order to gain insight into the
 161 mechanisms of NO_y chemistry during winter haze events.
 162
 163

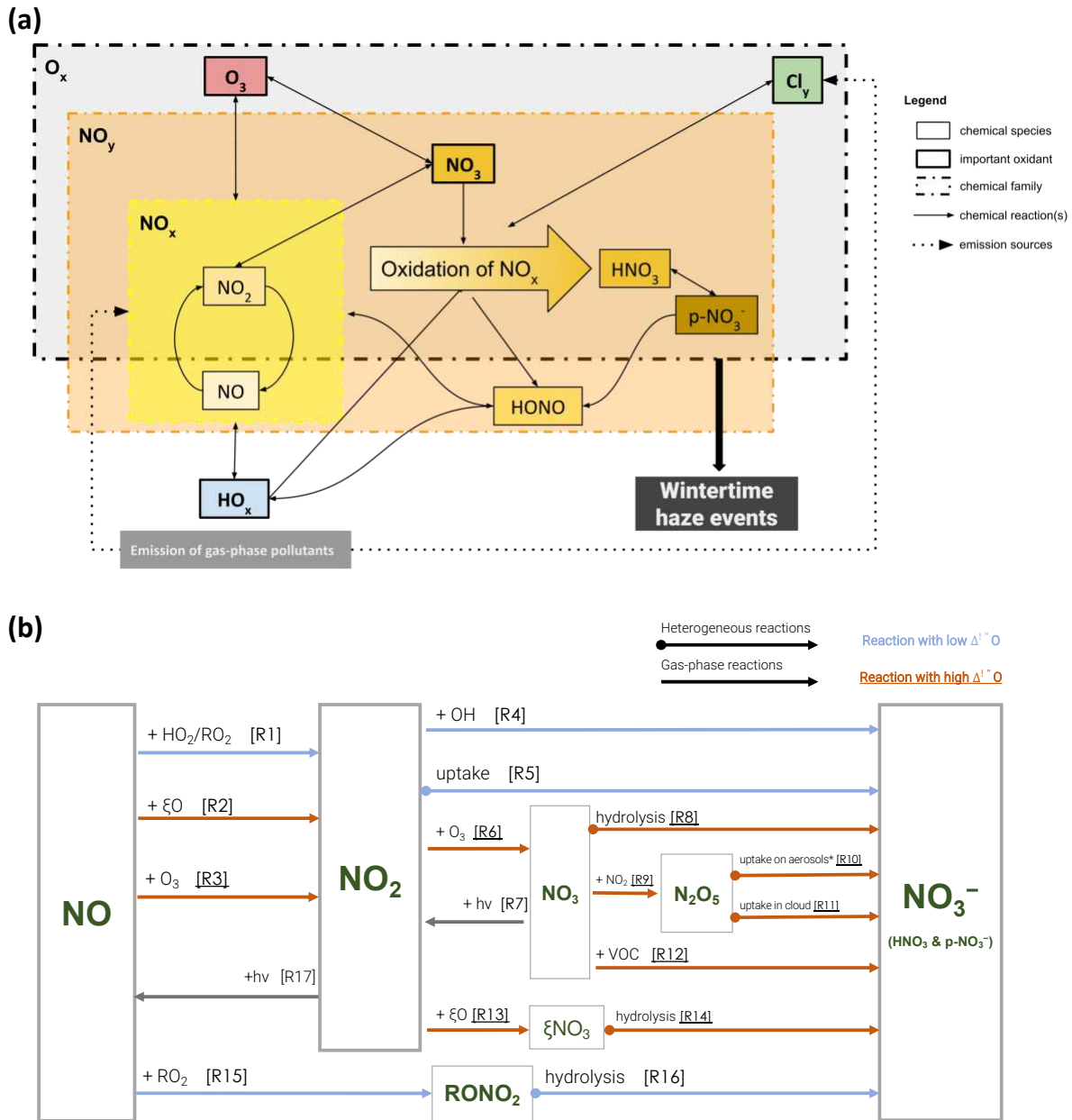


Figure 1. Simplified schematic of the chemistry of nitrate production in urban air. 1(a) is the schematic of the coupling of nitrate production and the emission of gas-phase pollutants, the NO_y chemical family, the budget of odd oxygen species, and PM pollution. 1(b) is the schematic of nitrate production pathways in the model and important intermediate species from the oxidation of NO_x to NO₃⁻ ([NO₃⁻] = [HNO₃] + [p-NO₃⁻]). “ξ” stands for the

halogens (Cl/ Br/I), while “VOC” stands for volatile organic compounds. N_2O_5 uptake on aerosols (R10) can undergo two possible pathways, depending on the chloride content in the aerosol. The chemical equation and other details of the reactions R1 to R17 can be found in Table S1.

2 Data and Methods

2.1 Measurements of $\Delta^{17}\text{O}(\text{NO}_3^-)$, aerosol, and trace gases during Beijing in winter 2014-15

Observations of $\Delta^{17}\text{O}(\text{NO}_3^-)$ in Beijing were previously published in He et al. (2018), Y. Wang et al. (2019), and W. Song et al. (2020) and are briefly described here. Most of the aerosol samples were collected in the Beijing metropolitan area from October 2014 to January 2015 and later sent to IsoLab at the University of Washington for isotopic analysis. The location of the measurement sites is shown in Figure S1(a). He et al. (2018) and W. Song et al. (2020) used collection intervals of about 12 hours for each aerosol sample, whereas Y. Wang et al. (2019) used 23 hours. The aerosol filters collected both HNO_3 and p-NO_3^- , so the observed $\Delta^{17}\text{O}(\text{NO}_3^-)$ contains $\Delta^{17}\text{O}$ signals from both species (He et al., 2018). We compute the daily mean of $\Delta^{17}\text{O}(\text{NO}_3^-)$ from these published measurements and obtain a dataset with 51 data points between 1 October 2014 and 15 January 2015.

To evaluate the modeled concentration of $\text{PM}_{2.5}$, p-NO_3^- , NO_2 , and ozone in Beijing, we use measurements of these species reported in He et al. (2018), Y. Wang et al. (2019), and W. Song et al. (2020). We also consider similar measurements at other Beijing air-quality stations that are operated by the China Ministry of Ecology and Environment as a complementary dataset (location of these sites are shown in Figure S1(a)). These air-quality measurements are publicly available on <https://quotsoft.net/air> (last accessed on 26 January 2021).

2.2 GEOS-Chem 3-D Chemical Transport Model simulations

We use the three-dimensional global chemical transport model GEOS-Chem (version 12.7.0; hereafter GC) to simulate the evolution of haze events in winter 2014-15. This version of the GC model code is accessible from <https://doi.org/10.5281/zenodo.3634864> (last accessed on 26 January 2021). The model considers detailed HO_x - NO_x -VOC-ozone-halogen-aerosol chemistry in the troposphere (Fisher et al., 2018; Kasibhatla et al., 2018; Sherwen et al., 2017; X. Wang et al., 2019, 2020). The Fast-JX module in GC calculates aerosol radiative effects and photolysis rates (Eastham et al., 2014; Neu et al., 2007). The partitioning between the HNO_3 and p-NO_3^- is determined by an aerosol thermodynamic equilibrium module ISORROPIA II (Fountoukis & Nenes, 2007). The deposition schemes for trace gases and aerosols in GC are described in Y. Wang et al. (1998), H. Liu et al. (2001), L. Zhang et al. (2001), and Jaeglé et al. (2018). Since GC uses offline meteorological data to drive simulations by design, it will not be able to capture the feedback processes involving aerosol-boundary interaction, which can potentially be important during haze events in wintertime East China (Huang et al., 2020). Earlier versions of GC have also been used to investigate NO_x and PM pollution in metropolitan areas (e.g., Jaeglé et al., 2018; Shah et al., 2020).

The NO_y chemistry in GC has been updated substantially in recent versions of the model. Holmes et al. (2019) modified the uptake coefficients for NO_2 , NO_3 , and N_2O_5 on different aerosols based on recent laboratory studies. In particular, $\gamma(\text{NO}_2)$ on sulfate-nitrate-ammonium (SNA) aerosol has been set to 5×10^{-6} , which is a factor-of-20 reduction compared to the previous work. The latest versions of GC also incorporated the uptake of NO_2 , NO_3 and N_2O_5 in

211 cloud droplets, following the entrainment-limited scheme described in Holmes et al. (2019) for
212 partly cloudy conditions. For the uptake of N_2O_5 on SNA aerosol, the latest version of GC now
213 considers the inhibiting effects of organic coating through the parametrization described in
214 McDuffie et al. (2018), which was built on top of the Bertram and Thornton (2009) scheme to
215 calculate the reaction probability of N_2O_5 on aerosol. Particulate-nitrate photolysis described in
216 Kasibhatla et al. (2018) is currently an optional feature in GC and is switched off by default. For
217 gas-phase NO_y chemistry, the latest updates include the reactions of C1-C3 alkyl nitrate, as
218 described in Fisher et al. (2018). While the previous studies independently showed that these
219 chemistry updates improved the representation of NO_y in the model, no study to date has yet
220 examined the combined effects of these updates on model simulations of wintertime haze events
221 in China.

222
223 In this study, we use version 12.7.0 of GC as our “base model”. Driven by GEOS-FP
224 meteorological data assimilation products with a native horizontal resolution of $0.25^\circ \times 0.3125^\circ$
225 and 72 vertical levels, the base simulation was run at a coarser spatial resolution (4° latitude \times 5°
226 longitude and 47 vertical levels) to attain global coverage. We also performed nested-grid
227 regional simulations for East Asia at a higher horizontal resolution (0.25° latitude \times 0.3125°
228 longitude) by using output from the corresponding global simulations as boundary conditions
229 (See Figure S1(b) and S1(c) for grid size and boundaries). The model simulates the mixing of
230 chemical species in the planetary boundary layer using the non-local mixing scheme from Lin
231 and McElroy (2010). Anthropogenic emissions of reactive gases and aerosols over the United
232 States, Canada, Asia, and Africa are from the regional emissions inventories EPA/NEI2011,
233 APEI, MIX, and DICE-Africa, respectively (M. Li et al., 2017; Marais & Wiedinmyer, 2016).
234 NO_x emissions from MEIC (the emission inventory for China in MIX framework) between 2005
235 and 2018 have recently been validated by the satellite retrievals of NO_2 columns in Shah et al.
236 (2020) and showed a good agreement. Emissions in the rest of the world are from the
237 Community Emissions Data System (CEDS) inventory (Hoesly et al., 2018). Biomass burning
238 emissions are from the Global Fire Emissions Database (GFED 4.1s) (van der Werf et al., 2017).
239 Lightning- NO_x emissions in the model are estimated based on a satellite lightning climatology
240 described in Murray et al. (2012). Soil- NO_x emissions are estimated offline using the algorithm
241 described in Hudman et al. (2012). The model simulation period is from August 2014 to January
242 2015, in which the first two months are used for “spinning-up” the model. To address the
243 uncertainty in NO_y chemistry, we conduct a series of model sensitivity experiments at 4° latitude
244 \times 5° longitude resolution. The detailed configurations for these simulations are described in
245 Section 3.2.2 and Text S2 in SI.

246
247

248 **2.3 Calculation of $\Delta^{17}\text{O}(\text{NO}_3^-)$ in model simulations**

249
250 Following the approach of Alexander et al. (2020), we use local chemical production rates to
251 calculate $\Delta^{17}\text{O}(\text{NO}_3^-)$, by which we assume that $\Delta^{17}\text{O}(\text{NO}_3^-)$ is controlled by local NO_x cycling
252 and nitrate production (See Figure S2). This method works well for intense haze events in
253 wintertime North China Plain, where most NO_3^- is produced locally over the North China Plain
254 (See Figure S3). The $\Delta^{17}\text{O}$ in tropospheric ozone ($\Delta^{17}\text{O}(\text{O}_3)$) is assumed to be 26‰ based on
255 recent measurements (Vicars & Savarino, 2014). We assume that only the terminal oxygen atom
256 of ozone is transferred during oxidation reactions; hence the $\Delta^{17}\text{O}$ value of the oxygen atom

257 transferred is equal to 39‰ ($= \frac{3}{2} \times 26\text{‰}$, denoted as $\Delta^{17}\text{O}(\text{O}_3^*)$) (Morin et al., 2011). For
 258 calculation of $\Delta^{17}\text{O}(\text{NO}_2)$, we assume isotopic equilibration during the daytime for all nitrate
 259 production pathways. The longer lifetime of NO_x in wintertime North China Plain (≈ 21 to 27
 260 hours estimated by Shah et al. (2020)) suggests that NO_x oxidation rates are slow enough to
 261 make this a reasonable assumption. Figure S2 also shows the assumed $\Delta^{17}\text{O}(\text{NO}_3^-)$ values for
 262 each nitrate formation pathway in the model.

263
 264

265 **2.4 Other metrics for evaluating NO_y chemistry**

266

267 In addition to $\Delta^{17}\text{O}$, we also use the concentration and speciation of the odd oxygen family (O_x)
 268 to evaluate the performance of the model in simulating NO_y chemistry. In theory, O_x includes all
 269 the chemical species that cycle with ozone and atomic oxygen in the atmosphere via
 270 photochemical reactions and is highly coupled with the local nitrate production (Bates & Jacob,
 271 2020; Lu et al., 2019; Womack et al., 2019).

272

273 Here, we define total O_x as the weighted sum of ozone and other species that cycle with ozone
 274 and atomic oxygen in the model:

275

$$276 \quad \text{O}_x \equiv \text{O}_3 + \text{NO}_2 + 2\text{NO}_3 + 3\text{N}_2\text{O}_5 + \text{HNO}_3 + \text{p-NO}_3^- + \text{PANs} + \text{RONO}_2 + \text{HNO}_4 + \xi\text{O} \\
 277 \quad + \xi\text{NO}_2 + 2\xi\text{NO}_3 + \sum_{n=2}^5 n\xi_2\text{O}_n + 20\xi\text{O}$$

278

279 where $\xi = \text{Br, Cl, or I}$. Our definition of O_x is very similar to the one used in Bates and Jacob
 280 (2020), except that we (1) include p-NO_3^- and (2) exclude the short-lived radical species (e.g.,
 281 $\text{O}(^1\text{D})$ and Criegee intermediates) that have a negligible impact on total O_x abundances. We
 282 consider p-NO_3^- to be an O_x member because of the rapid equilibrium partitioning between
 283 HNO_3 and p-NO_3^- on fine-model aerosol and the potential importance of renoxification in urban
 284 air from the photolysis of p-NO_3^- (Bao et al., 2018; Kasibhatla et al., 2018; Y. Liu et al., 2019;
 285 Ye et al., 2017). Womack et al. (2019) also included p-NO_3^- in their definition of generalized
 286 odd oxygen family. While GC can simulate and output all the species listed in our definition of
 287 O_x , most of the measurements in Beijing only include the concentration of O_3 , NO_2 , and p-NO_3^-
 288 (with possible interference of HNO_3 , as explained in Section 2.1). The incomplete observations
 289 of O_x only have minor effects on our model-observation comparison because O_3 , NO_2 , and p-
 290 NO_3^- are the dominant ($>95\%$) O_x species in wintertime Beijing in the model (See more detailed
 291 analysis in Section 3.1). We denote the sum of O_3 , NO_2 , and p-NO_3^- as $\text{O}_{x,\text{major}}$.

292

293 Since the speciation of O_x is sensitive to NO_y chemistry, we also compare the ratio of different
 294 O_x species in the observations and the model simulations. In particular, we compute the nitrogen
 295 oxidation ratio (NOR) using the mixing ratios of NO_2 and NO_3^- :

296

$$297 \quad \text{NOR} \equiv \frac{[\text{NO}_3^-]}{[\text{NO}_3^-] + [\text{NO}_2]} = \frac{[\text{p-NO}_3^-] + [\text{HNO}_3]}{[\text{p-NO}_3^-] + [\text{HNO}_3] + [\text{NO}_2]}$$

298

299 NOR ranges from 0 (complete absence of NO_3^-) to 1 (complete oxidation of all NO_2). This
300 dimensionless ratio indicates the efficiency of the oxidation of NO_x and is less prone to absolute
301 errors in simulating NO_x concentrations (such as uncertainties in emissions). NOR has been
302 widely used in the analysis of nitrate formation mechanisms in other studies (e.g., He et al.,
303 2018; P. Liu et al., 2020; Shi et al., 2019; Xu et al., 2019).

304

305

306 **2.5 Haze-regime categorization**

307

308 To facilitate our analysis of the relationships between the chemistry metrics and the intensity of
309 haze events, we categorize the data into four haze regimes according to the surface $\text{PM}_{2.5}$
310 concentration: "light haze" ($[\text{PM}_{2.5}] \leq 75 \mu\text{g m}^{-3}$), "moderate haze" events ($75 \mu\text{g m}^{-3} < [\text{PM}_{2.5}] \leq$
311 $150 \mu\text{g m}^{-3}$), "severe haze" events ($150 \mu\text{g m}^{-3} < [\text{PM}_{2.5}] \leq 225 \mu\text{g m}^{-3}$), and "extreme haze"
312 events ($[\text{PM}_{2.5}] > 225 \mu\text{g m}^{-3}$) (See Table S2 for the frequency of different haze regimes). For
313 the observations, we compute the average of daily mean $[\text{PM}_{2.5}]$ observed at the Beijing air-
314 quality stations (both urban and suburban stations, 22 stations in total) to determine the haze
315 regime of a particular day. The inter-station average $[\text{PM}_{2.5}]$ can better reflect the intensity of
316 regional haze events than the single-station measurements. For model data, we use the modeled,
317 mean surface $[\text{PM}_{2.5}]$ over the Beijing gridbox in coarse-resolution simulations. It is noted that
318 the choice of this categorization does not imply the existence of statistically significant
319 differences between chemical metrics in different haze regimes or abrupt shifts in NO_y chemistry
320 at regime boundaries (where $[\text{PM}_{2.5}] = 75, 150, \text{ or } 225 \mu\text{g m}^{-3}$). Instead, this categorization is
321 merely used for illustrating and communicating some general trends in NO_y chemistry as haze
322 intensifies. Similar categorizations have also been adopted in other studies of nitrate pollution in
323 Beijing (e.g., Fu et al., 2020; He et al., 2018; P. Liu et al., 2020). When we are referring to
324 patterns that are seen across multiple haze regime, the terms "intense haze" ($[\text{PM}_{2.5}] > 75 \mu\text{g m}^{-3}$)
325 and "more intense haze" ($[\text{PM}_{2.5}] > 150 \mu\text{g m}^{-3}$) are sometimes used.

326

327

328 **3 Results**

329

330 **3.1 Observations of $\Delta^{17}\text{O}(\text{NO}_3^-)$ in Beijing**

331

332 A compilation of all available $\Delta^{17}\text{O}(\text{NO}_3^-)$ observations reveals a positive relationship between
333 $\Delta^{17}\text{O}(\text{NO}_3^-)$ and $\text{PM}_{2.5}$ concentration in Beijing during winter 2014-15 (Figure 2). The median of
334 $\Delta^{17}\text{O}(\text{NO}_3^-)$ increases from 26.1‰ in light haze to 31.5‰ in extreme haze (Figure 2b). Similar
335 positive relationships between $\Delta^{17}\text{O}(\text{NO}_3^-)$ and $[\text{PM}_{2.5}]$ have also been reported in He et al.
336 (2018) and Y. Wang et al. (2019). The positive relationship can still be seen when we analyze
337 daytime and nighttime measurements separately (Figure S4). The lack of strong diurnal
338 variability in $\Delta^{17}\text{O}(\text{NO}_3^-)$ in observations is consistent with the long lifetime of NO_x in
339 wintertime North China Plain shown by previous modeling studies (e.g., Shah et al., 2020). The
340 higher $\Delta^{17}\text{O}(\text{NO}_3^-)$ measured in intense haze indicates that the relative importance of high- $\Delta^{17}\text{O}$
341 pathways involving O_3 increases with $\text{PM}_{2.5}$ concentration.

342

343 Figure 2 also shows that the variability of $\Delta^{17}\text{O}(\text{NO}_3^-)$ is larger on days with lower $[\text{PM}_{2.5}]$. The
344 standard deviation (s.d.) of $\Delta^{17}\text{O}(\text{NO}_3^-)$ decreases from 3.7‰ in light haze to 1.7‰ intense haze.

345 The observed smaller variability of $\Delta^{17}\text{O}(\text{NO}_3^-)$ in intense haze may be explained by the weaker
 346 ventilation and the overwhelming contribution of nitrate from local production (See Figure S3).
 347 We also note that very high variability in $\Delta^{17}\text{O}(\text{NO}_3^-)$ is only seen in the light-haze observations
 348 from Y. Wang et al. (2019) (the corresponding s.d. is 3.9‰). Observations in He et al. (2018) and
 349 W. Song et al. (2020) show a similar variability in $\Delta^{17}\text{O}$ (the overall s.d. are 1.6‰ and 1.4‰,
 350 respectively) and do not contain the low $\Delta^{17}\text{O}(\text{NO}_3^-)$ values (<26‰) reported by Y. Wang et al.
 351 (2019). Thus, we focus our analysis more on intense haze when the observations from all three
 352 studies are in better agreement on the magnitude and variability in $\Delta^{17}\text{O}(\text{NO}_3^-)$.
 353

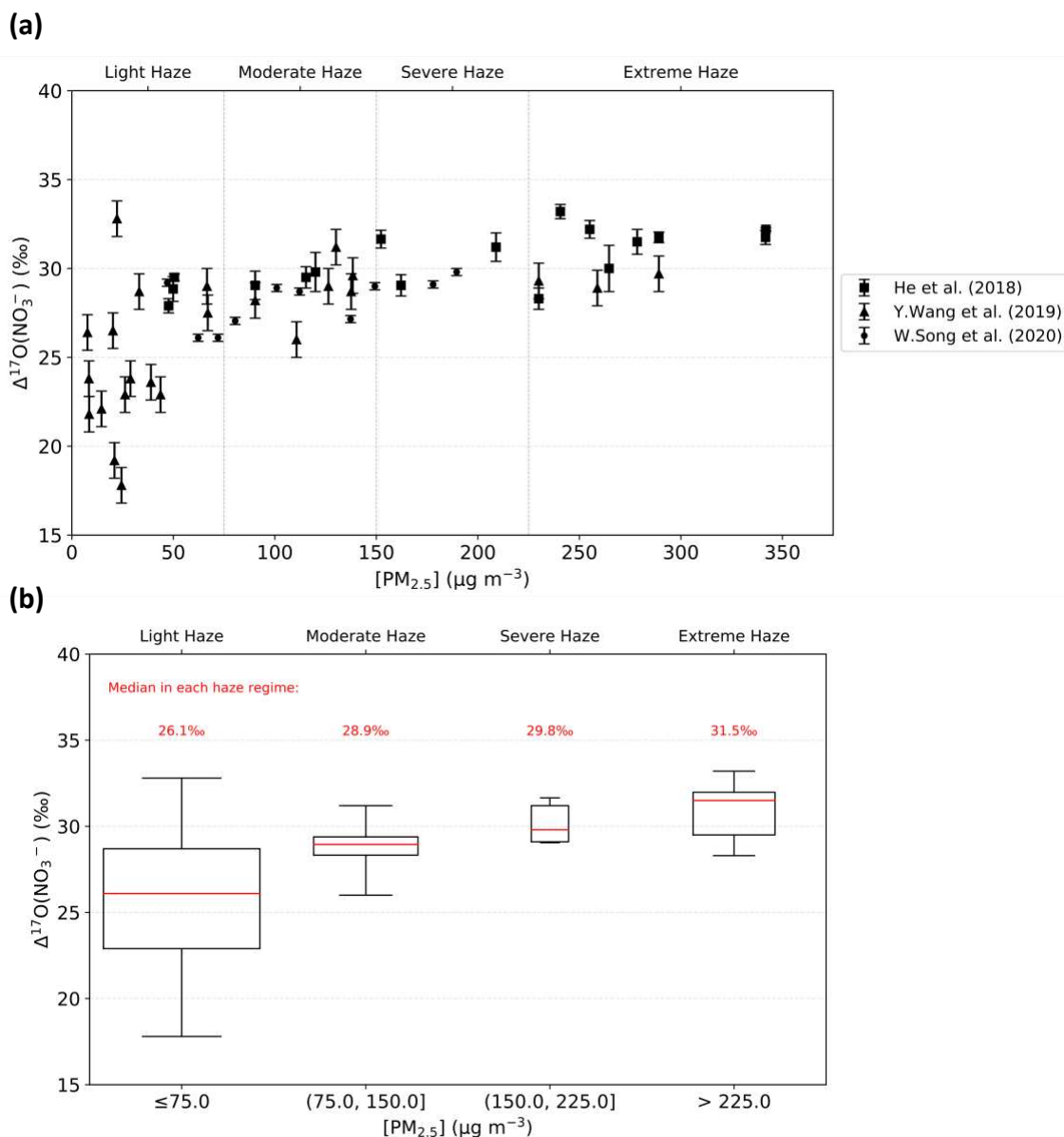


Figure 2. Observed relationship between $\Delta^{17}\text{O}(\text{NO}_3^-)$ and $\text{PM}_{2.5}$ concentration. The scatter plot in 2(a) shows the daily-average measurements in He et al. (2018) (squares), Y. Wang et al. (2019) (triangles), and W. Song et al. (2020) (circles). The number in red above each box shows the value of the median of $\Delta^{17}\text{O}(\text{NO}_3^-)$ in each haze regime. The error bars

represent the $\pm 2\sigma$ standard deviation uncertainty range for the $\Delta^{17}\text{O}$ measurements. The box plot in 2(b) shows the statistics of the observed $\Delta^{17}\text{O}(\text{NO}_3^-)$ in each haze regime. The red line indicates the median; the top and the bottom of the box indicate the 75th percentile and the 25th percentile, respectively; the whiskers indicate the maximum and the minimum. The width of boxes scales with the number of samples in each haze regime.

354

355

356 **3.2 Model Results**

357

358 **3.2.1 Base Model**

359

360 Figure 3 compares the magnitude of modeled and observed $\Delta^{17}\text{O}(\text{NO}_3^-)$ in Beijing in intense
 361 haze. While the modeled median $\Delta^{17}\text{O}(\text{NO}_3^-)$ in moderate haze (29.5‰) and severe haze
 362 (29.1‰) lie within the range of observations, most of the modeled $\Delta^{17}\text{O}(\text{NO}_3^-)$ in extreme haze
 363 (median = 27.3‰) are lower than the minimum value in the observations (28.3‰). The lower
 364 $\Delta^{17}\text{O}(\text{NO}_3^-)$ in extreme haze compared to moderate and severe haze means the base model
 365 predicts a negative relationship between $\Delta^{17}\text{O}(\text{NO}_3^-)$ and $[\text{PM}_{2.5}]$ in intense haze (Figure 3),
 366 which is the opposite relationship shown in the observations. Modeled median $\Delta^{17}\text{O}(\text{NO}_3^-)$ in
 367 moderate haze is 2.2‰ higher than that in extreme haze. Lower $\Delta^{17}\text{O}(\text{NO}_3^-)$ in extreme haze
 368 cannot be explained by the modeled difference in $\Delta^{17}\text{O}(\text{NO}_2)$, of which the median changes by
 369 less than 0.5‰ across different types of haze events (Figure S5).

370

371 The base model also cannot reproduce a sufficient amount of O_x , the observed O_x speciation, nor
 372 the observed NOR in Beijing in intense haze (Figure 4 and Figure 5). Modeled $[\text{O}_x, \text{major}]$ in
 373 intense haze is 36% lower than the observations on average. The bias in modeled $[\text{O}_x]$ in the
 374 North China Plain is mainly caused by an underestimate of $[\text{NO}_2]$ and $[\text{O}_3]$ (Figure 4, and more
 375 discussion in Section 4.2). In extreme haze, the base model underestimates the mean of $[\text{NO}_2]$
 376 and $[\text{O}_3]$ by 55% and 54%, respectively. The large model-observation discrepancy in $[\text{NO}_2]$
 377 cannot be explained by the long-known interference of NO_z species (members in the NO_y family
 378 that are not NO or NO_2) in chemiluminescence-based measurements (Lamsal et al., 2008; Reed
 379 et al., 2016), because both our model (see Figure S6) and other observations suggest that non-
 380 NO_3^- gas-phase NO_z species' (e.g., PAN) concentration is small in comparison with $[\text{NO}_x]$ in
 381 wintertime in Beijing (S. Chen et al., 2020; B. Zhang et al., 2017; G. Zhang et al., 2020; H.
 382 Zhang et al., 2014). The underestimate of NO_2 leads to a modeled overestimate of NOR (0.33) in
 383 intense haze compared to the observations (0.21). The discrepancy between modeled and
 384 observed NOR increases with $[\text{PM}_{2.5}]$. In extreme haze, the modeled median NOR (0.50) is
 385 higher than the observed maximum (0.47) (Figure 5).

386

387 The base model's bias in $\Delta^{17}\text{O}(\text{NO}_3^-)$, $[\text{O}_x]$, and NOR persists even when a higher horizontal
 388 spatial resolution is used. The range of the chemical metrics increases with model resolution, but
 389 the median and the mean remain largely unchanged (Figures 3, 4 and 5). The relationship
 390 between modeled $\Delta^{17}\text{O}(\text{NO}_3^-)$ and $[\text{PM}_{2.5}]$ is still negative in intense haze (Figure 3). Moreover,
 391 the extended range of modeled $\Delta^{17}\text{O}(\text{NO}_3^-)$ still cannot capture the maximum and minimum in
 392 observations. A similar model underestimate of mean $[\text{O}_x]$ during intense haze events is seen in
 393 both the regional-level and the site-level comparison (Figure 4 and Figure S7). The nested-grid
 394 simulation predicts a slightly lower median NOR (-0.01 , -0.05 , and -0.07 in moderate, severe,

395 and extreme haze, respectively), but the modeled NOR is still too high compared to the
 396 observations (Figure 5). The comparison between nested-grid and global simulations suggests
 397 that low horizontal spatial resolution is not the fundamental cause for the model's bias in NO_y
 398 chemistry over the North China Plain. Comparison of observed and modeled mixed layer depths
 399 also suggests that the bias in the thickness of vertical mixing layer is not a cause of the model
 400 biases in trace gas concentrations (See Figure S8).

401
 402 In the base simulation, the major low- $\Delta^{17}\text{O}$ pathways in Beijing are gas-phase oxidation of NO_2
 403 by OH and NO_2 uptake on aerosols, which contribute 34.4% and 19.0 % to nitrate production on
 404 average over winter 2014-15, respectively (Figure 6). The major high- $\Delta^{17}\text{O}$ pathways are N_2O_5
 405 uptake on aerosols (33.6%) and clouds (11.3%) (Figure 6). The relative importance of high- $\Delta^{17}\text{O}$
 406 pathways and low- $\Delta^{17}\text{O}$ pathways remains at around a ratio of 1:1 from light haze to severe haze
 407 events. In extreme haze, the contribution from NO_2 uptake increases sharply to 35.9% and
 408 becomes higher than N_2O_5 uptake on aerosols and clouds (30.0%), resulting in relatively low
 409 values of $\Delta^{17}\text{O}(\text{NO}_3^-)$ (Figure 6).

410
 411 The model-observation comparison of the $\Delta^{17}\text{O}(\text{NO}_3^-)$ in extreme haze suggests that the standard
 412 version of GC either overestimates the contribution of low- $\Delta^{17}\text{O}$ pathways and/or underestimates
 413 the contribution of high- $\Delta^{17}\text{O}$ pathways as $\text{PM}_{2.5}$ increases. In the base simulation, the modeled
 414 reduction in $\Delta^{17}\text{O}(\text{NO}_3^-)$ in extreme haze is driven by an increase in NO_2 uptake rate and a
 415 decrease in N_2O_5 uptake on aerosols (Figure 6a), suggesting that the modeled rate of NO_2 uptake
 416 is too high and/or the rate of N_2O_5 uptake is too low in extreme haze. It is also possible that the
 417 model underestimates the contribution of the other high- $\Delta^{17}\text{O}$ nitrate production pathways, such
 418 as reactions between NO_3 and VOCs (Figure 1b, R12) and the hydrolysis of halogen nitrates
 419 (Figure 1b, R14). However, further analysis and model sensitivity simulations suggest that either
 420 these reactions are negligible and/or cannot resolve the model biases in the chemical metrics
 421 because of the limited supply of NO_3 and N_2O_5 in intense haze (Refer to Text S1 and Text S2.2 in
 422 SI).

423

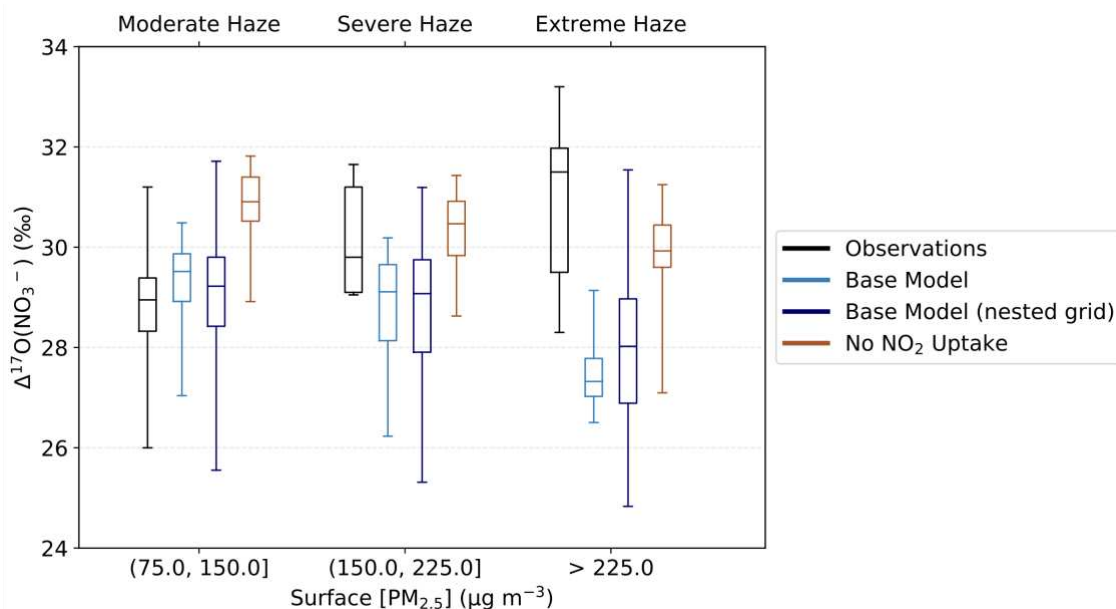


Figure 3. Comparison of $\Delta^{17}\text{O}(\text{NO}_3^-)$ in observations and model simulations under different haze regimes.

424

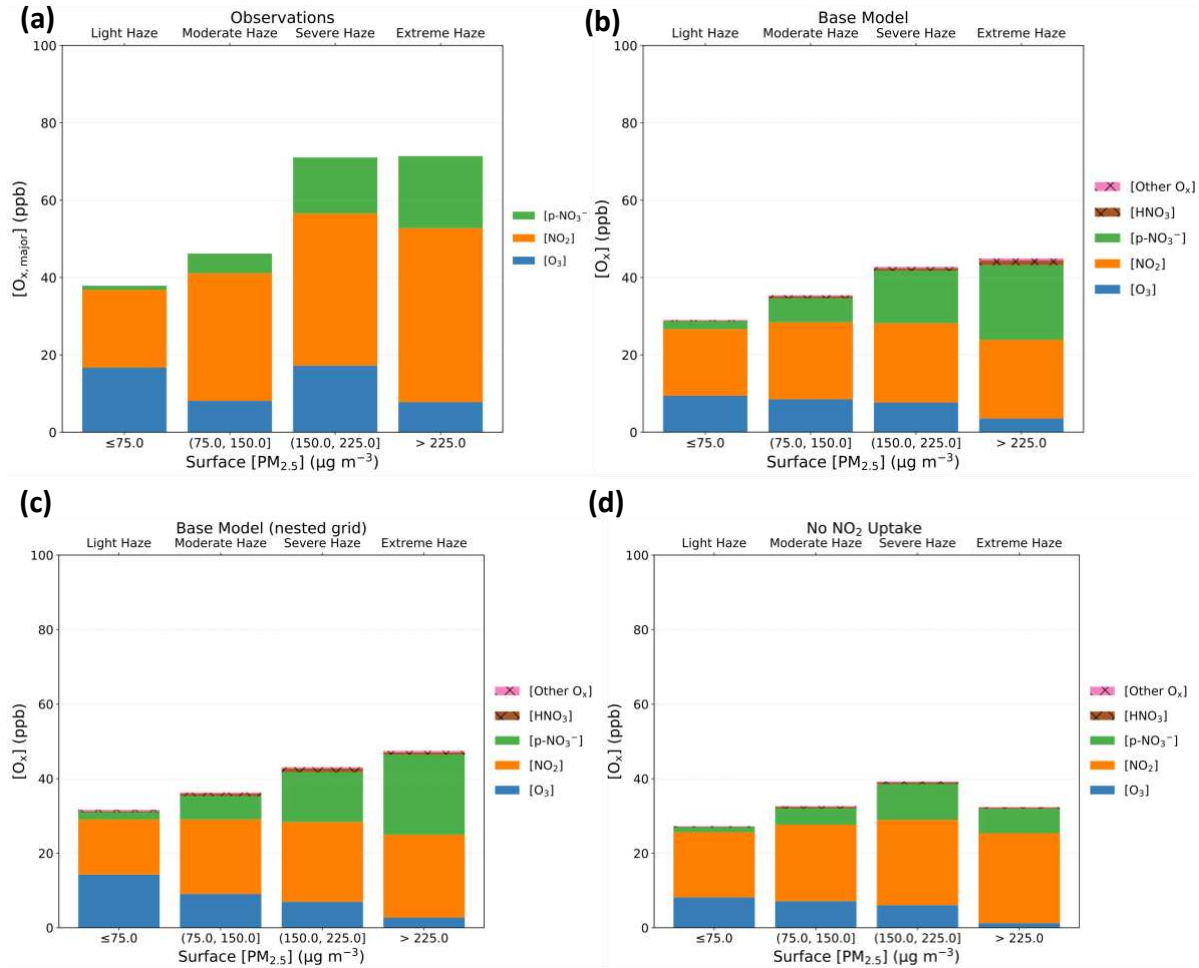


Figure 4. Concentration and speciation of O_x under different haze regimes in (a) observations, (b) base simulation, (c) nested-grid base simulation, (d) No NO₂ Uptake simulation. Hatching (x-filled bars) indicates the O_x species that were not measured at the observation sites.

425

426

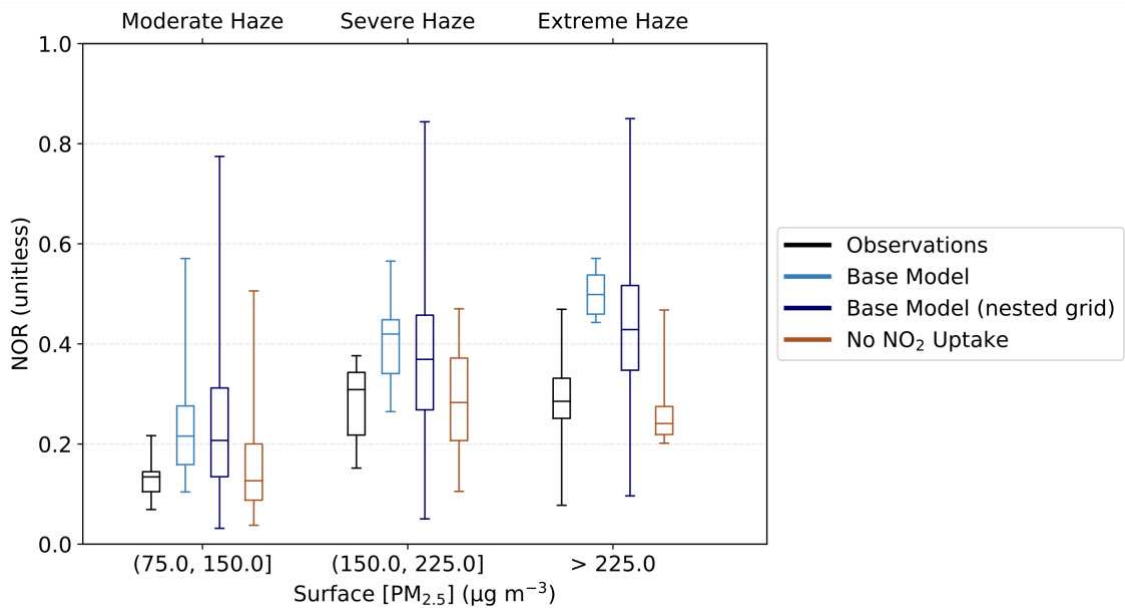


Figure 5. Comparison of nitrogen oxidation ratio (NOR) in observations and model simulations under different haze regimes.

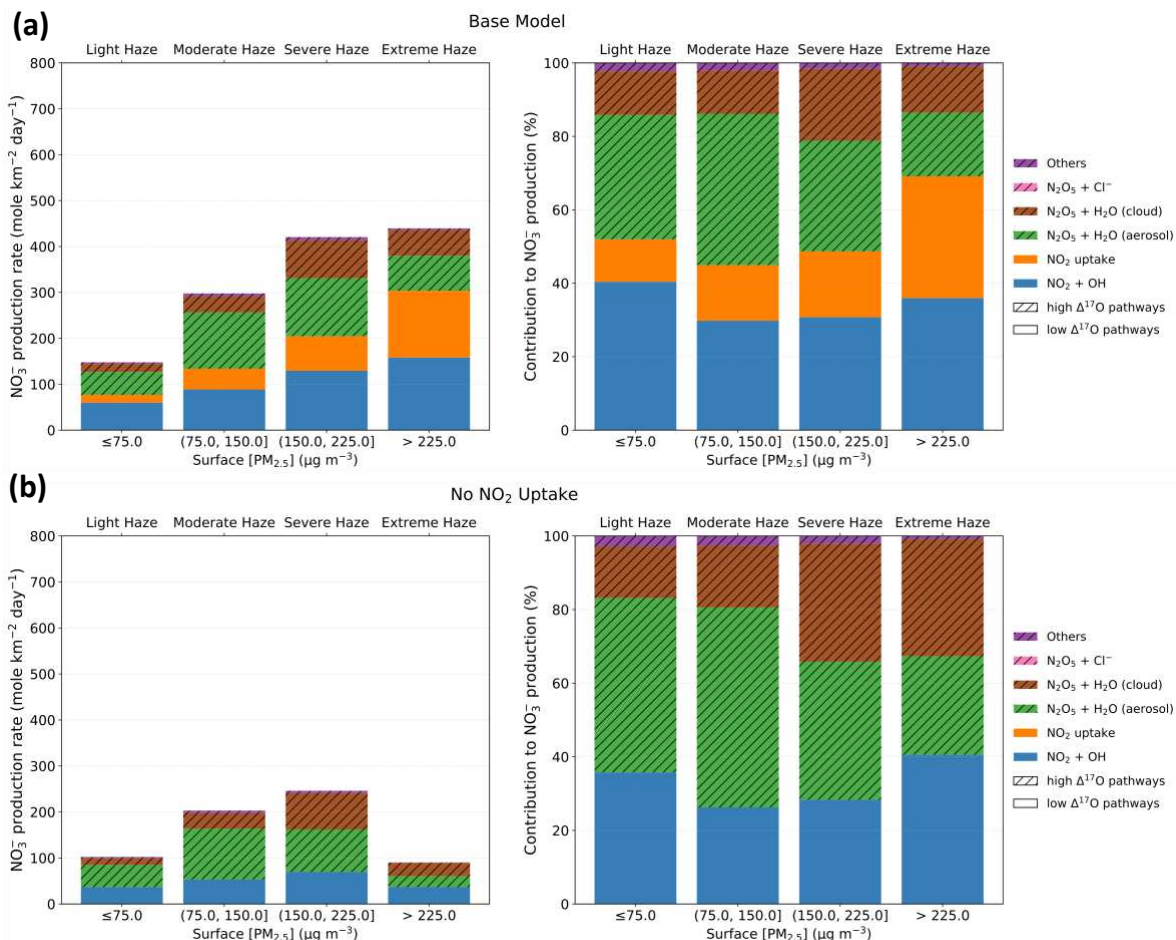


Figure 6. Average rate of different near-surface nitrate production pathways (left) and their relative contribution to nitrate formation in Beijing under different haze regimes (right) in (a) the base simulation and (b) No NO₂ Uptake simulation. “Near-surface” is defined as the sum over the ten lowest vertical levels in model, which on average corresponds to the altitudes between 0 to 1300 m. Hatching (// -filled bars) indicates high- $\Delta^{17}\text{O}$ pathways.

428

429

3.2.2 No-NO₂-uptake model simulation

431

432 An overestimate of NOR combined with the models’ low bias in $\Delta^{17}\text{O}$ suggests an overestimate
 433 of NO₂ uptake (a low- $\Delta^{17}\text{O}$ heterogeneous pathway). Although a high bias in NOR could also
 434 suggest an underestimate of renoxification, a model sensitivity study allowing for efficient
 435 photolysis of p-NO₃⁻ shows that this explanation cannot resolve the model biases (Refer to Text
 436 S2.1 in SI). To evaluate the role of NO₂ uptake on the three chemistry metrics, we perform a
 437 sensitivity simulation in which the reaction is removed from the model by setting the uptake
 438 coefficients of NO₂ uptake on all types of aerosol and clouds to zero (i.e., $\gamma(\text{NO}_2) = 0$).

439

440 Without NO₂ uptake, the model predicts higher $\Delta^{17}\text{O}(\text{NO}_3^-)$ relative to the base model simulation
 441 under all haze regimes (Figure 3). The average increase in modeled $\Delta^{17}\text{O}(\text{NO}_3^-)$ in intense haze
 442 is 1.5 %, and the largest increase is found in extreme haze: the modeled median $\Delta^{17}\text{O}(\text{NO}_3^-)$
 443 increases by 2.6 % compared to the base simulation. Most of the modeled $\Delta^{17}\text{O}(\text{NO}_3^-)$ in

444 extreme haze now lie inside the range of observations. The simulation without NO₂ uptake
445 predicts the median $\Delta^{17}\text{O}(\text{NO}_3^-)$ in extreme haze to be 29.9‰, which is closer to the
446 observations (31.5‰). However, the model now overestimates the $\Delta^{17}\text{O}(\text{NO}_3^-)$ in moderate haze.
447 The median $\Delta^{17}\text{O}(\text{NO}_3^-)$ in moderate haze in the model is 30.9‰, which is 2.0‰ higher than the
448 observations. Similar to the base simulation, the simulation without NO₂ uptake predicts a
449 decrease in $\Delta^{17}\text{O}(\text{NO}_3^-)$ as [PM_{2.5}] increases. The negative relationship is driven by the sharp
450 decrease in the rate of N₂O₅ production and nitrate production via N₂O₅ uptake in extreme haze
451 (Figure 6).

452
453 The model without NO₂ uptake shows better agreement with observations of O_x speciation and
454 NOR but still underestimates the total O_x concentration (Figure 4 and Figure 5). The average
455 NOR in intense haze in the model is 0.22, which is very close to the observations (0.21). The
456 modeled NOR in extreme haze spans within the observed range for all haze regimes (Figure 5).
457 Modeled [O_x] is not sensitive to the change in NO₂ uptake, except in extreme haze. [O_x] in
458 extreme haze decreases from 41.0 ppb in the base simulation to 34.6 ppb in the simulation with
459 no NO₂ uptake. This worsens the underestimate of modeled [O_x].

460
461 The reduction in NOR relative to the base model simulation is due to a reduction in the nitrate-
462 production rate in all haze regimes, but especially during extreme haze (Figure 6). This is driven
463 mainly by the absence of NO₂ uptake as a nitrate-production pathway, but also due to a decrease
464 in nitrate production via NO₂ + OH. The decrease in nitrate production via NO₂ + OH is driven
465 by the lack of HONO production from NO₂ uptake, the photolysis of which was a major source
466 of OH in the model. The rate of N₂O₅ uptake remains relatively unchanged, except for a decrease
467 during extreme haze (Figure 7). This increases the relative importance of N₂O₅ uptake resulting
468 in an increase in $\Delta^{17}\text{O}(\text{NO}_3^-)$ during all haze regimes compared to the base model, especially
469 during more intense haze events.

470
471 The results from the simulation without NO₂ uptake demonstrates that model discrepancies in
472 $\Delta^{17}\text{O}(\text{NO}_3^-)$ and O_x as seen in the base simulation cannot be solely explained by the uncertainty
473 in the efficiency of NO₂ uptake. Even when we completely eliminate the contribution of nitrate
474 production from the NO₂ uptake pathway, the existing high- $\Delta^{17}\text{O}$ pathways in the model still
475 cannot contribute enough to reproduce the observed range of $\Delta^{17}\text{O}(\text{NO}_3^-)$ in severe haze and
476 extreme haze. This model sensitivity simulation also shows that the supply of [NO₂] is not a rate-
477 limiting factor for N₂O₅ uptake in Beijing. As less NO₂ is converted into NO₃⁻ due to the absence
478 of NO₂ uptake pathway, the modeled [O₃] becomes more depleted as [NO_x] increases (Figure 4
479 and Figure S6). In the presence of excess NO_x, the low [O₃] in the model slows down the
480 production of NO₃ radicals via NO₂ + O₃, which ultimately limits the rate of N₂O₅ production via
481 NO₂ + NO₃ and nitrate production via N₂O₅ uptake. Compared with the base simulation, the
482 simulation without NO₂ uptake predicts lower N₂O₅ production and lower nitrate production via
483 N₂O₅ uptake on aerosols and clouds in extreme haze (Figure 7), further supporting that O₃ is the
484 limiting factor for N₂O₅ production and uptake.

485
486

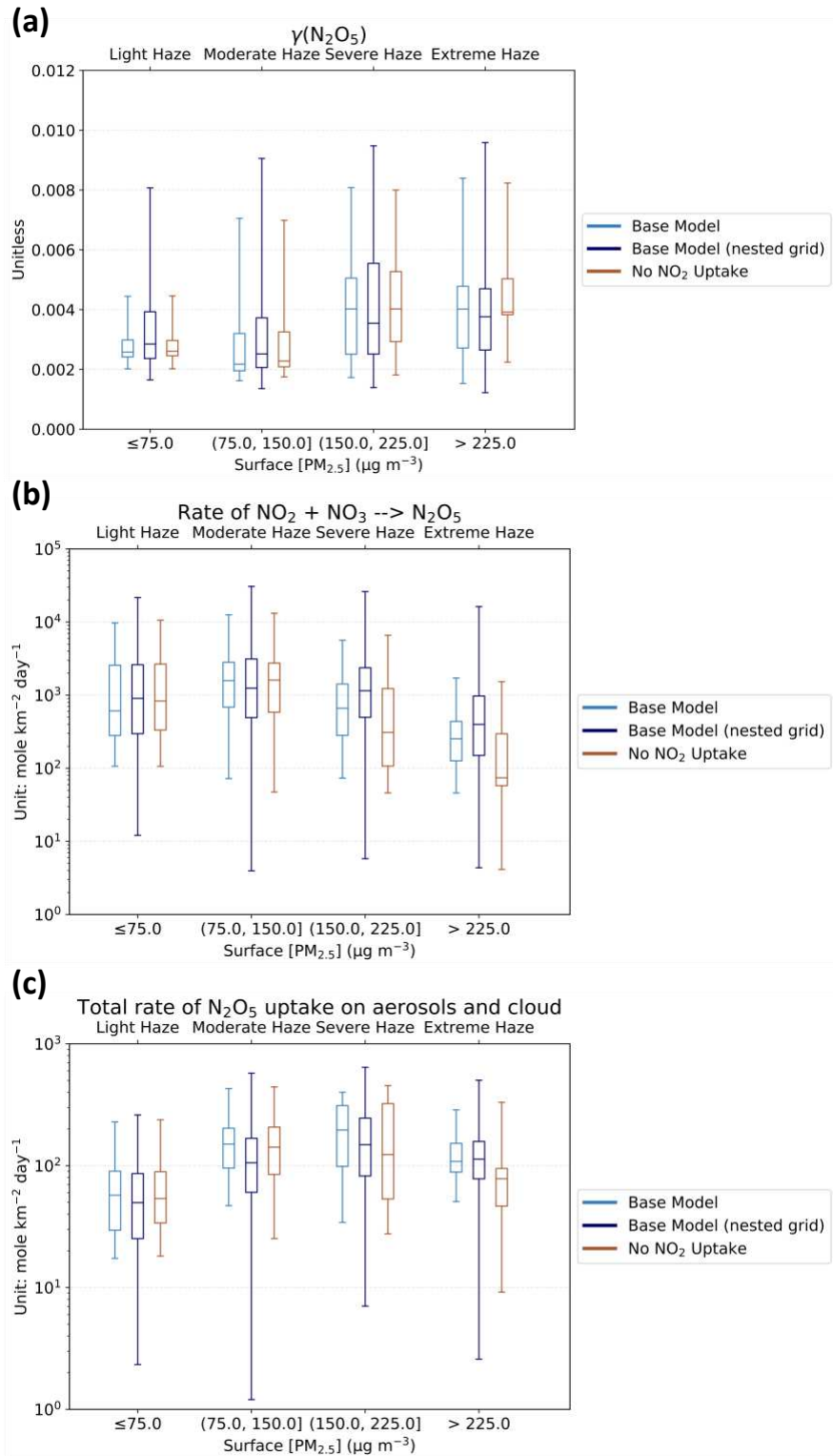


Figure 7. Factors controlling the near-surface rate of nitrate production via N_2O_5 hydrolysis in simulations and their dependence on $[\text{PM}_{2.5}]$. 7(a) shows the average uptake coefficient of N_2O_5 on aerosols. 7(b) shows the average rate of N_2O_5 production. 7(c) shows the average total rate of N_2O_5 uptake on aerosols and cloud.

488 4 Discussion

490 4.1 Model sensitivity to uncertainties in NO₂ uptake on aerosol

491
492 The model results presented in Section 3 and Text S2 show that modeled NOR and $\Delta^{17}\text{O}(\text{NO}_3^-)$
493 are most sensitive to NO₂ uptake. In NO_x-rich air, we expect to see positive relationships
494 between [HO_x] and [O₃] because of their coupling via the cycling of NO_x (Bates & Jacob, 2020).
495 As modeled O₃ concentration increases, NO more likely reacts with O₃ to produce NO₂, as a
496 result, more HO_x becomes available for other reactions, including nitrate production, and vice
497 versa. The competing effects of HO_x- and ozone-related nitrate-production pathways explain
498 why modeled $\Delta^{17}\text{O}(\text{NO}_3^-)$ is not very sensitive to changes in various chemical parameters, with
499 the exception of $\gamma(\text{NO}_2)$. NO₂ uptake, which carries a low- $\Delta^{17}\text{O}$ signature, is the only important
500 nitrate-production pathway in the base model that converts NO₂ into NO₃⁻ without involving
501 HO_x or ozone directly (Figure 1b). Additional model simulations increasing the HONO yield
502 resulting from NO₂ uptake on aerosol to 100%, as well as model simulations including various
503 combinations of the three model sensitivity studies described in Section 3.2 and Text S2, further
504 show that $\Delta^{17}\text{O}(\text{NO}_3^-)$ and NOR are most sensitive to $\gamma(\text{NO}_2)$ (Figure S9 and Figure S10). The
505 extra HONO produced from NO₂-uptake yielding 100% HONO increases OH and the rate of
506 NO₂ + OH and simultaneously promotes nitrate production via N₂O₅ uptake through HO_x-O₃
507 coupling effects (See Figure S11), but the modeled [O_x] is still low compared to the observations
508 (Figure S12). Among all the model simulations performed, only those with $\gamma(\text{NO}_2) = 0$ improve
509 model agreement with both observed $\Delta^{17}\text{O}(\text{NO}_3^-)$ and NOR during more intense haze events
510 (Figure S9 and Figure S10).

511
512 In addition to the isotopic constraints, results from some laboratory and field studies also support
513 the choice of a lower $\gamma(\text{NO}_2)$. The current GC parametrization sets $\gamma(\text{NO}_2, \text{black carbon})=10^{-4}$,
514 which is 20 times higher than $\gamma(\text{NO}_2, \text{SNA})$. Laboratory studies of NO₂(g) uptake on soot or
515 carbonaceous surfaces suggested that heterogeneous reactions can rapidly consume the organic
516 adsorbates and/or surface groups (Ammann et al., 1998; Bröske et al., 2003; Gerecke et al.,
517 1998; Kalberer et al., 1999; Kleffmann et al., 1999), with rates of NO₂ uptake decreasing to
518 negligible levels within minutes to hours (Gerecke et al., 1998; Kalberer et al., 1999; Kleffmann
519 et al., 1999). For SNA aerosols, laboratory studies by F. Tan et al. (2016) and F. Tan et al. (2017)
520 found that the rate of NO₂ uptake decreases with increasing RH when aerosols contain CaCO₃
521 due to formation of insoluble CaSO₄·nH₂O on aerosol surfaces at higher RH. A potential
522 suppressing effect of high-RH conditions on NO₂ uptake may help to explain the positive
523 relationship between $\Delta^{17}\text{O}(\text{NO}_3^-)$ and [PM_{2.5}] in observations. P. Liu et al. (2020) used the RH-
524 dependence of NO₂ uptake to explain the negative relationship between NOR and RH when RH
525 is above 60% in their Beijing observations. However, we cannot replicate their finding using our
526 observations, which show a positive relationship between NOR and RH across all RH conditions
527 (Figure S13). While some studies suggested that the heterogeneous reactions between NO₂ and
528 SO₂ are important during wintertime haze events (e.g., Cheng et al., 2016; J. Wang et al., 2020),
529 analysis of sulfate $\Delta^{17}\text{O}$ observations by Shao et al. (2019) showed that these reactions contribute
530 less than 2% to heterogeneous formation of sulfate based on isotope observations in Beijing
531 during the time period studied here. Given the large uncertainties of NO₂ uptake under
532 atmospheric conditions and its large influence on nitrate production, HONO production, and [O_x]

533 in extreme haze, future studies should investigate the dominant mechanisms of NO₂ uptake on
534 ambient aerosols and seek additional observational constraints during more intense haze events.

537 **4.2 Possible causes of modeled underestimate in wintertime [O_x] in the North China Plain** 538 **and their potential influence on NO_y chemistry**

539
540 The model bias in wintertime ozone is critical for the simulation of [O_x] and nitrate production
541 via N₂O₅ uptake. NO₂ and ozone are the major components of [O_x], but the base model
542 underestimates their concentration in Beijing, especially during intense haze events. Modeled
543 [NO_x] increases with [PM_{2.5}] in Beijing, and NO becomes the primary NO_x species in severe and
544 extreme haze (Average [NO]/[NO_x] ratios are 0.55 and 0.66, respectively, in the base model. See
545 Figure S6). The high [NO]/[NO_x] ratio on more polluted days is also evident in other wintertime
546 observations in Beijing (Lu et al., 2019; Jiaqi Wang et al., 2017; G. Zhang et al., 2020). Under
547 NO_x-saturated regime, the daytime cycling of NO and NO₂ is mainly controlled by the rates of
548 NO + O₃ reaction (R3, a.k.a. ozone titration) and NO₂ photolysis. As predicted by the Leighton
549 Relationship, [NO₂]/[NO] ratio is linearly proportional to [O₃] at photochemical steady state.
550 From this basic theoretical perspective, the model bias in wintertime ozone should at least partly
551 explain the underestimate in [NO₂] in our simulations. The actual NO_x-O₃ relationship may
552 deviate from Leighton's prediction because of the complicated interaction between aerosols and
553 radiation, which can affect the photolysis of NO₂ and O₃ (Hollaway et al., 2019; W. Wang et al.,
554 2019). As explained in Section 3.2, low [O₃] can also limit nitrate production via N₂O₅ uptake in
555 NO_x-rich air. Since ozone is a secondary pollutant that plays a central role in tropospheric
556 chemistry, the formation of ozone is inevitably sensitive to many different chemical processes.
557 The particulate-nitrate-photolysis and chlorine-chemistry simulations show improvement in
558 reproducing [O₃] in intense haze in Beijing compared to the base simulation, but none of the
559 proposed updates to NO_y and Cl_y chemistry investigated here can completely correct the model's
560 overall bias in O_x in Beijing (See Figure S12 and Text S2). In this section, we discuss other
561 chemical processes that may explain the modeled underestimate in wintertime [O₃] and [O_x].

562 563 564 **4.2.1 Aerosol uptake of HO₂ radicals**

565
566 The uptake of HO₂ radicals on aerosols has been suggested as a key process in driving the
567 observed trends of ozone in China in the 2010s (J. Li et al., 2018; K. Li, Jacob, Liao, Shen, et al.,
568 2019; K. Li, Jacob, Liao, Zhu, et al., 2019). Aerosols can scavenge gas-phase HO₂ radicals
569 reducing [HO_x] and inhibiting ozone production. As pollution-control policies in China have
570 reduced ambient [PM_{2.5}] in the 2010s, less HO₂ is scavenged by aerosols, resulting in increases
571 in the ozone production efficiency. This theory on HO_x-O₃-aerosol interactions is consistent with
572 the increasing trend of summertime ozone observed in China (K. Li, Jacob, Liao, Shen, et al.,
573 2019; K. Li, Jacob, Liao, Zhu, et al., 2019).

574
575 Despite the potential impacts of aerosol uptake of HO₂ on ozone in urban air, the efficiency of
576 this chemical process is still highly uncertain and may strongly depend on the content of aqueous
577 transition-metal ions, the acidity, and the size of the aerosol (Guo et al., 2019; Mao et al., 2013;
578 Thornton & Abbatt, 2005). To estimate the largest possible influence of HO₂ uptake on model

579 bias in $[O_x]$ in intense haze, we consider the extreme case of $\gamma(HO_2) = 0$ on all aerosols (Denote
580 as no HO_2 uptake simulation). Disabling the uptake of HO_2 on aerosols increases the modeled
581 median $[O_{x, major}]$ by 9.5% in intense haze, but this is smaller than the corresponding change
582 resulting from introducing p- NO_3^- photolysis into the model (+24%) (See Figure S12 and Text
583 S2). The model still fails to reproduce the high level of $[O_x]$ in observations in intense haze. The
584 overall effect of HO_2 uptake on NOR and $\Delta^{17}O(NO_3^-)$ are small in comparison with the models
585 with $\gamma(NO_2) = 0$ (See Figure S9 and Figure S10). Our simulation results show that the
586 uncertainty in $\gamma(HO_2)$ is not of primary importance to the model bias in simulating $[O_x]$, NOR,
587 and $\Delta^{17}O(NO_3^-)$ in Beijing.

588
589

590 **4.2.2 Wintertime emissions of volatile organic compounds in the North China Plain**

591

592 The roles of VOCs in nitrate production have been highlighted in recent studies of nitrate
593 pollution in urban air (Fu et al., 2020; He et al., 2018; Shah et al., 2020; W. Song et al., 2020; Y.
594 Wang et al., 2019; Womack et al., 2019). In Text S1, we showed that the direct effects of VOCs
595 on nitrate formation are likely small in wintertime Beijing. However, VOCs can still modulate
596 nitrate production rates by influencing ozone formation (Huang et al., 2021; Womack et al.,
597 2019). VOCs accelerate the production of O_3 in NO_x -rich urban air. Reduction in VOC emissions
598 has been proposed as a key strategy for mitigating wintertime nitrate pollution in Beijing and in
599 Utah (Lu et al., 2019; Womack et al., 2019). Because of the potential importance of [VOCs] in
600 nitrate production during intense haze events, we investigate the model bias in simulating
601 wintertime [VOCs] in Beijing and examine whether a bias in [VOCs] can explain the model-
602 observation discrepancy in terms of $[O_x]$.

603

604 Emitted from biomass burning and fossil fuels, aromatic compounds are often considered to be
605 the largest contributor to ozone formation in metropolitan areas in China (J. Sun et al., 2018; Yan
606 et al., 2017; D. Yu et al., 2020). The concentration of aromatics in general positively correlates
607 with $[PM_{2.5}]$ in the model (Table S3), consistent with observations in the North China Plain (C.
608 Liu et al., 2017; Sheng et al., 2018; J. Sun et al., 2018). However, the model underestimates the
609 concentration of aromatics compared to the observations, except for xylene. The mean
610 concentration of benzene in the base simulation is lower than the wintertime observations in
611 Beijing by a factor of 2 (see Table S3). Le et al. (2020) showed that a 30% increase in the
612 emissions of VOCs from conventional anthropogenic sources can increase the wintertime $[O_3]$
613 by about 10% in their model. Model bias in wintertime VOC emissions from industry and
614 transportation could be an important reason for the underestimate of modeled $[O_x]$ during intense
615 haze events.

616

617 Recent studies suggested that the manufacture and consumption of volatile chemical products
618 (VCPs) can be an overlooked anthropogenic VOC-emission source in air-quality models (e.g.,
619 McDonald et al., 2018). Throughout the product life cycle, these VCPs emit many complex
620 VOCs, including $C \geq 4$ alkanes, alcohols, and terpenes, and may account for about half of the
621 VOC reactivity with OH in Los Angeles (McDonald et al., 2018). Comparison of the
622 concentration of these VCP-related VOCs in the base simulation with wintertime observations in
623 Beijing shows a model underestimate of the concentration of alcohols, monoterpenes, and $C \geq 4$
624 alkanes in Beijing (See Table S3). However, without more observational constraints on the fluxes

625 and speciation of VCP emissions in the North China Plain and their dependencies on atmospheric
626 conditions, it is hard to conclude whether the model bias in $[O_x]$ can be reduced by including
627 emissions of VCPs in the simulations.

628
629

630 **4.3 Examination of the non-linearity in nitrate chemistry**

631

632 The weak response of particulate nitrate and other secondary aerosols to the reduction in NO_x
633 emissions has been noted in studies of the long-term trends in wintertime air quality (e.g., H. Li
634 et al., 2019; Shah et al., 2018; Xu et al., 2019), and more recently, in studies of air quality during
635 the COVID-19 pandemic (Diamond & Wood, 2020; Huang et al., 2021; Le et al., 2020; Y. Sun
636 et al., 2020). An astonishing example of the complexity of this NO_x -aerosol relationship can be
637 found in the observations in the North China Plain from January to March in year 2020.

638 Following a 40-60% reduction in the NO_x emissions over the North China Plain caused by
639 COVID-19 lockdown, observed $[PM_{2.5}]$, paradoxically, increased by 50% or more at several
640 stations near Beijing (Huang et al., 2021; Le et al., 2020). Studies suggested that the surge is
641 mostly driven by the production of secondary aerosols, including p- NO_3^- (Huang et al., 2021; Le
642 et al., 2020).

643

644 Many studies attributed the persistence of high levels of p- NO_3^- to the non-linearity in
645 atmospheric chemistry, but they hypothesized different mechanisms. Shah et al. (2018)
646 suggested that NO_x and SO_2 emission reductions over the eastern United States has resulted in a
647 gradual increase in aerosol alkalinity, which favors HNO_3 -to-p- NO_3^- conversion and increases
648 the fraction of p- NO_3^- in wintertime aerosols. We denote the non-linearity originated from the
649 sensitivity of p- NO_3^- to aerosol-pH as the ‘alkalinity-limited mechanism’. In contrast, studies in
650 China observed an increase in $[O_3]$ and production of secondary aerosols following the emission
651 reductions during COVID-19 lockdown, which is likely caused by a reduction in ozone titration
652 (Huang et al., 2021; Le et al., 2020). The enhancement in $[O_3]$ increases the oxidizing capacity of
653 the lower troposphere and promotes the production of secondary aerosols (Fu et al., 2020; Huang
654 et al., 2021; Le et al., 2020). We denote the non-linearity arising from the sensitivity of nitrate to
655 NO_x -VOCs-ozone chemistry as the ‘ozone-limited mechanism’.

656

657 To examine the relevance of ozone-limited mechanism in our model simulations of nitrate
658 production, we analyze the relationship between nitrate production rate, $[O_3]$, and $[NO_x]$ during
659 intense haze events for Beijing (Figure 8). It is noted that the inter-model differences in our study
660 originates from the variations in the modeled chemistry. This is different from other studies like
661 Huang et al. (2021), where they focused on the effects of changing emissions. Although the
662 modeled $[O_3]$, $[NO_x]$, and nitrate production rate are considerably different among various
663 experiments, a positive relationship between nitrate production rate and $[O_3]$ during intense haze
664 events can be identified in all the simulations with $\gamma(NO_2) = 0$. In contrast, all these simulations
665 predict a negative relationship between the nitrate production rate and $[NO_x]$, which can be
666 attributed to the effects of ozone titration. The strong and positive correlation between the nitrate
667 production rate and $[O_3]$ predicted by our models is consistent with the theory of ozone-limited
668 mechanism. Meanwhile, our simulations also show that the partitioning between p- NO_3^- and
669 HNO_3 in Beijing is not sensitive to the intensity of haze events or the difference in NO_y
670 chemistry parametrization (See Figure S14). p- NO_3^- remains the dominant form of NO_3^- in all

671 cases. The model prediction is also consistent with the estimated high aerosol pH (4.5 ± 0.7) in
 672 wintertime Beijing, which can be explained by the high NH_3 abundance in observations (Ding et
 673 al., 2019). Our model simulations confirm the importance of ozone-limited mechanism in
 674 wintertime North China Plain and show that the positive relationship between $[\text{O}_3]$ and nitrate
 675 production rate during intense haze events is robust regardless of the uncertainty in modeled NO_y
 676 chemistry after $\gamma(\text{NO}_2)$ is set to 0.
 677

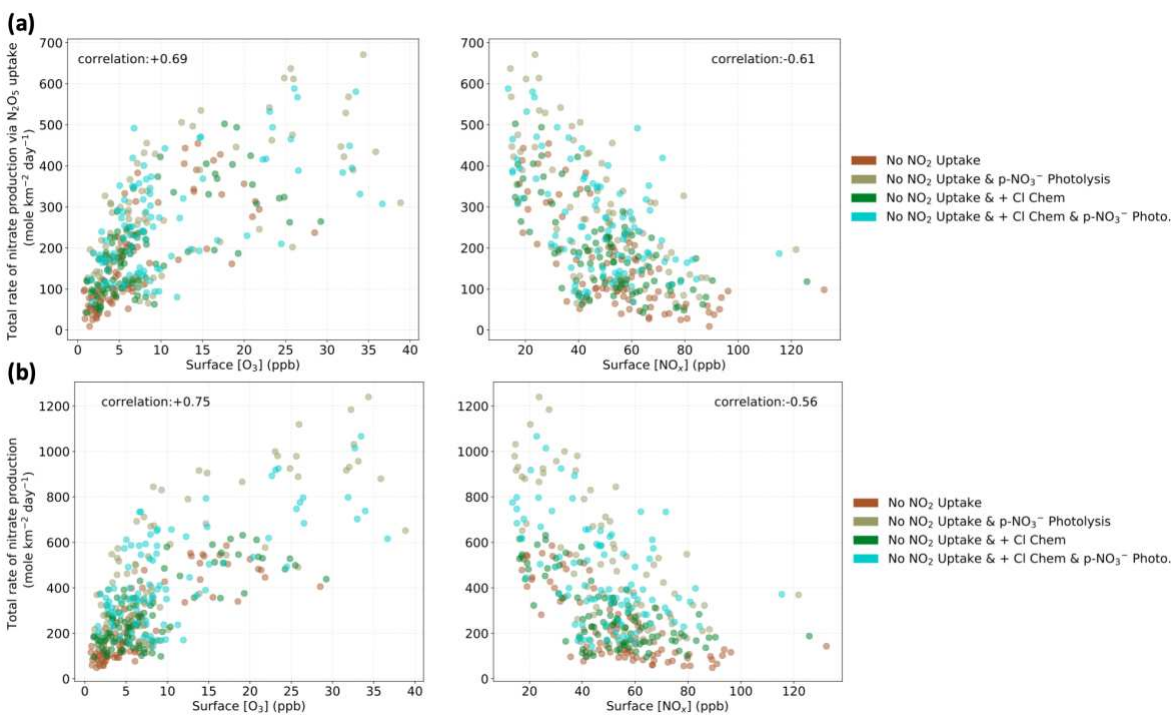


Figure 8. The relationship between $[\text{O}_3]$, $[\text{NO}_x]$, the rate of nitrate production via N_2O_5 uptake (8a), and the total rate of nitrate production (8b) during intense haze events in simulations without NO_2 uptake on aerosols. The correlation coefficients shown in the figure are calculated using data from all the four model experiments. All the estimated linear-regression slopes are different from 0 at the 95% significance level.

678

679

680 5 Conclusions and Implications

681

682 By analyzing the observations of $\Delta^{17}\text{O}(\text{NO}_3^-)$, NOR, and O_x in Beijing during winter 2014-15
 683 and results from a global and regional chemical transport model, we examine the mechanisms for
 684 nitrate production in wintertime North China Plain and how the underlying chemical processes
 685 vary with the intensity of haze events. $\Delta^{17}\text{O}(\text{NO}_3^-)$ indicates the dominance of high- $\Delta^{17}\text{O}$
 686 oxidants (e.g., ozone) to low- $\Delta^{17}\text{O}$ oxidants (e.g., OH and RO_2) during NO_x -to- NO_3^- conversion,
 687 while NOR and O_x provide information about the efficiency of NO_y oxidation and the oxidizing
 688 capacity of the air. In intense haze, the base model underestimates $\Delta^{17}\text{O}(\text{NO}_3^-)$ and $[\text{O}_x]$ in
 689 Beijing by -0.86% and -36% , respectively, but overestimates NOR by $+0.12$. To investigate
 690 the relationship between model bias and uncertainty in chemistry, we perform model sensitivity
 691 experiments by varying several key parameters in NO_y chemistry. Our analysis suggests a model

692 overestimate in NO₂-uptake rate on aerosols and the underestimate in wintertime ozone may
693 explain the model biases.

694
695 Our model sensitivity simulations show that modeled $\Delta^{17}\text{O}(\text{NO}_3^-)$ and NOR during highly
696 polluted conditions are most sensitive to the parametrization of NO₂ uptake on aerosols. The
697 $\Delta^{17}\text{O}(\text{NO}_3^-)$ observations in Beijing and its relationship with [PM_{2.5}] suggest that the rate of NO₂
698 uptake is likely too high in the model, yielding too high nitrate- and HONO-production rates in
699 more intense haze. Model simulations without NO₂ uptake better reproduce the observed
700 $\Delta^{17}\text{O}(\text{NO}_3^-)$ and NOR in Beijing under high-PM_{2.5} conditions. A NO₂ uptake mechanism that is
701 suppressed by high RH may explain the positive relationship between $\Delta^{17}\text{O}(\text{NO}_3^-)$ and [PM_{2.5}] in
702 observations, but the supporting evidence for such a mechanism is currently inconclusive.
703 Further laboratory and field studies are needed to constrain the reaction probability of NO₂ on
704 ambient aerosols, with a focus on its role in nitrate and HONO formation.

705
706 Our simulations also reveal that nitrate production is largely limited by ozone during intense
707 haze events in wintertime North China Plain. After accounting for the uncertainty in NO₂ uptake
708 on aerosols, our analysis suggests that N₂O₅ uptake in aerosols and clouds is the dominant
709 mechanism for nitrate production in wintertime Beijing. Under high-NO_x-high-PM_{2.5} conditions,
710 [O₃] modulates N₂O₅ production and, subsequently, the rate of nitrate production via N₂O₅
711 uptake. The base model underestimates [O₃] and [O_x] during wintertime haze events. Uncertainty
712 in heterogeneous chemical processes, such as renoxification via nitrate photolysis or ClNO₂
713 production and the scavenging of HO_x by aerosols, may contribute to the model bias in
714 wintertime O_x, but our simulations show that adjusting related chemistry parameters cannot
715 remove the bias even under extreme scenarios, suggesting processes other than chemistry (e.g.,
716 emissions of VCPs and feedbacks involving aerosol-boundary-layer interaction) may play a
717 more important role. Both the reduction in [PM_{2.5}] and NO_x emissions have been shown to lead
718 to increases in [O₃] in the North China Plain (Huang et al., 2021; Le et al., 2020; K. Li, Jacob,
719 Liao, Zhu, et al., 2019). Nitrate production rates may continue to increase as long as [O₃]
720 increases despite decreases in [NO_x], creating a negative feedback that reduces the effectiveness
721 of air pollution reduction strategies. Policies that result in a reduction of ambient O₃
722 concentrations, possibly through reductions in VOC emissions, will also reduce the formation of
723 nitrate and its contribution to PM_{2.5} during wintertime haze events.

724
725

726 **Acknowledgments and Data**

727 This work was supported by funding from the National Science Foundation (NSF) to B.A. (Grant
728 AGS 1644998). Y.C.C. acknowledges helpful discussions with Brian Boys from Dalhousie
729 University, Men Xia from the Hong Kong Polytechnic University, and Wei Zhou from the
730 Chinese Academy of Sciences. P.Z.H acknowledges the funding support from the Natural
731 Science Foundation of Anhui Province, China (Grant 2008085QD184). C.D.H acknowledges
732 the funding support from National Aeronautics and Space Administration (NASA) (Grant
733 NNX16A157G). L.J. acknowledges the funding support from NSF (Grant AGS-1901786). J.A.T.
734 acknowledges the funding support from NSF (Grant AGS-1652688). Z.Q.X. acknowledges the
735 funding support from the National Key Project of Ministry of Science and Technology of the
736 People's Republic of China (Grant 2016YFC0203302). Data used in this study is hosted in the

737 University of Washington's ResearchWorks Archive and can be accessed online
738 (<http://hdl.handle.net/1773/46927>).
739

740 **References**

- 741 Alexander, B., Sherwen, T., Holmes, C. D., Fisher, J. A., Chen, Q., Evans, M. J., & Kasibhatla,
742 P. (2020). Global inorganic nitrate production mechanisms: comparison of a global model
743 with nitrate isotope observations. *Atmospheric Chemistry and Physics*, 20(6), 3859–3877.
744 <https://doi.org/10.5194/acp-20-3859-2020>
- 745 Ammann, M., Kalberer, M., Jost, D. T., Tobler, L., Rössler, E., Piguet, D., et al. (1998).
746 Heterogeneous production of nitrous acid on soot in polluted air masses. *Nature*, 395(6698),
747 157–160. <https://doi.org/10.1038/25965>
- 748 An, Z., Huang, R.-J., Zhang, R., Tie, X., Li, G., Cao, J., et al. (2019). Severe haze in northern
749 China: A synergy of anthropogenic emissions and atmospheric processes. *Proceedings of*
750 *the National Academy of Sciences of the United States of America*, 116(18), 8657–8666.
751 <https://doi.org/10.1073/pnas.1900125116>
- 752 Bao, F., Li, M., Zhang, Y., Chen, C., & Zhao, J. (2018). Photochemical Aging of Beijing Urban
753 PM_{2.5}: HONO Production. *Environmental Science & Technology*, 52(11), 6309–6316.
754 <https://doi.org/10.1021/acs.est.8b00538>
- 755 Bates, K. H., & Jacob, D. J. (2020). An Expanded Definition of the Odd Oxygen Family for
756 Tropospheric Ozone Budgets: Implications for Ozone Lifetime and Stratospheric Influence.
757 *Geophysical Research Letters*, 47(4). <https://doi.org/10.1029/2019GL084486>
- 758 Bertram, T. H., & Thornton, J. A. (2009). Toward a general parameterization of N₂O₅ reactivity
759 on aqueous particles: The competing effects of particle liquid water, nitrate and chloride.
760 *Atmospheric Chemistry and Physics*, 9(21), 8351–8363. [https://doi.org/10.5194/acp-9-8351-](https://doi.org/10.5194/acp-9-8351-2009)
761 2009
- 762 Bröske, R., Kleffmann, J., & Wiesen, P. (2003). Heterogeneous conversion of NO₂ on secondary
763 organic aerosol surfaces: A possible source of nitrous acid (HONO) in the atmosphere?
764 *Atmospheric Chemistry and Physics*, 3(3), 469–474. <https://doi.org/10.5194/acp-3-469-2003>
- 765 Chen, S., Wang, H., Lu, K., Zeng, L., Hu, M., & Zhang, Y. (2020). The trend of surface ozone in
766 Beijing from 2013 to 2019: Indications of the persisting strong atmospheric oxidation
767 capacity. *Atmospheric Environment*, 242, 117801.
768 <https://doi.org/10.1016/j.atmosenv.2020.117801>
- 769 Chen, Y., Ebenstein, A., Greenstone, M., & Li, H. (2013). Evidence on the impact of sustained
770 exposure to air pollution on life expectancy from China's Huai River policy. *Proceedings of*
771 *the National Academy of Sciences of the United States of America*, 110(32), 12936–12941.
772 <https://doi.org/10.1073/pnas.1300018110>
- 773 Cheng, Y., Zheng, G., Wei, C., Mu, Q., Zheng, B., Wang, Z., et al. (2016). Reactive nitrogen
774 chemistry in aerosol water as a source of sulfate during haze events in China. *Science*
775 *Advances*, 2(12), e1601530. <https://doi.org/10.1126/sciadv.1601530>
- 776 Diamond, M. S., & Wood, R. (2020). Limited Regional Aerosol and Cloud Microphysical
777 Changes Despite Unprecedented Decline in Nitrogen Oxide Pollution During the February
778 2020 COVID-19 Shutdown in China. *Geophysical Research Letters*, 47(17).
779 <https://doi.org/10.1029/2020GL088913>
- 780 Ding, J., Zhao, P., Su, J., Dong, Q., Du, X., & Zhang, Y. (2019). Aerosol pH and its driving

- 781 factors in Beijing. *Atmospheric Chemistry and Physics*, 19(12), 7939–7954.
782 <https://doi.org/10.5194/acp-19-7939-2019>
- 783 Eastham, S. D., Weisenstein, D. K., & Barrett, S. R. H. (2014). Development and evaluation of
784 the unified tropospheric–stratospheric chemistry extension (UCX) for the global chemistry-
785 transport model GEOS-Chem. *Atmospheric Environment*, 89, 52–63.
786 <https://doi.org/10.1016/j.atmosenv.2014.02.001>
- 787 Fisher, J. A., Atlas, E. L., Barletta, B., Meinardi, S., Blake, D. R., Thompson, C. R., et al. (2018).
788 Methyl, Ethyl, and Propyl Nitrates: Global Distribution and Impacts on Reactive Nitrogen
789 in Remote Marine Environments. *Journal of Geophysical Research: Atmospheres*, 123(21),
790 12,429–12,451. <https://doi.org/10.1029/2018JD029046>
- 791 Fountoukis, C., & Nenes, A. (2007). *Atmospheric Chemistry and Physics ISORROPIA II: a*
792 *computationally efficient thermodynamic equilibrium model for K⁺-Ca²⁺-Mg²⁺-NH₄⁺*
793 *4-Na⁺-SO₄²⁻-4-NO₃⁻-3-Cl⁻-H₂O aerosols*. *Atmos. Chem. Phys* (Vol. 7). Retrieved from
794 www.atmos-chem-phys.net/7/4639/2007/
- 795 Fu, X., Wang, T., Gao, J., Wang, P., Liu, Y., Wang, S., et al. (2020). Persistent Heavy Winter
796 Nitrate Pollution Driven by Increased Photochemical Oxidants in Northern China.
797 *Environmental Science and Technology*, 54(7), 3881–3889.
798 <https://doi.org/10.1021/acs.est.9b07248>
- 799 Gaston, C. J., Thornton, J. A., & Ng, N. L. (2014). Reactive uptake of N₂O₅ to internally mixed
800 inorganic and organic particles: the role of organic carbon oxidation state and inferred
801 organic phase separations. *Atmospheric Chemistry and Physics*, 14(11), 5693–5707.
802 <https://doi.org/10.5194/acp-14-5693-2014>
- 803 Geng, L., Murray, L. T., Mickley, L. J., Lin, P., Fu, Q., Schauer, A. J., & Alexander, B. (2017).
804 Isotopic evidence of multiple controls on atmospheric oxidants over climate transitions.
805 *Nature*, 546(7656), 133–136. <https://doi.org/10.1038/nature22340>
- 806 Gerecke, A., Thielmann, A., Gutzwiller, L., & Rossi, M. J. (1998). The chemical kinetics of
807 HONO formation resulting from heterogeneous interaction of NO₂ with flame soot.
808 *Geophysical Research Letters*, 25(13), 2453–2456. <https://doi.org/10.1029/98GL01796>
- 809 Guo, J., Wang, Z., Tao Wang, & Zhang, X. (2019). Theoretical evaluation of different factors
810 affecting the HO₂ uptake coefficient driven by aqueous-phase first-order loss reaction.
811 *Science of The Total Environment*, 683, 146–153.
812 <https://doi.org/10.1016/j.scitotenv.2019.05.237>
- 813 He, P., Xie, Z., Chi, X., Yu, X., Fan, S., Kang, H., et al. (2018). Atmospheric Δ¹⁷O(NO₃⁻)
814 reveals nocturnal chemistry dominates nitrate production in Beijing haze. *Atmospheric*
815 *Chemistry and Physics*, 18(19), 14465–14476. <https://doi.org/10.5194/acp-18-14465-2018>
- 816 Hoesly, R. M., Smith, S. J., Feng, L., Klimont, Z., Janssens-Maenhout, G., Pitkanen, T., et al.
817 (2018). Historical (1750–2014) anthropogenic emissions of reactive gases and aerosols
818 from the Community Emissions Data System (CEDS). *Geoscientific Model Development*,
819 11(1), 369–408. <https://doi.org/10.5194/gmd-11-369-2018>
- 820 Hollaway, M., Wild, O., Yang, T., Sun, Y., Xu, W., Xie, C., et al. (2019). Photochemical impacts
821 of haze pollution in an urban environment. *Atmospheric Chemistry and Physics*, 19(15),
822 9699–9714. <https://doi.org/10.5194/acp-19-9699-2019>

- 823 Holmes, C. D., Bertram, T. H., Confer, K. L., Graham, K. A., Ronan, A. C., Wirks, C. K., &
824 Shah, V. (2019). The Role of Clouds in the Tropospheric NO_x Cycle: A New Modeling
825 Approach for Cloud Chemistry and Its Global Implications. *Geophysical Research Letters*,
826 *46*(9), 4980–4990. <https://doi.org/10.1029/2019GL081990>
- 827 Huang, X., Ding, A., Wang, Z., Ding, K., Gao, J., Chai, F., & Fu, C. (2020). Amplified
828 transboundary transport of haze by aerosol–boundary layer interaction in China. *Nature*
829 *Geoscience*, *13*(6), 428–434. <https://doi.org/10.1038/s41561-020-0583-4>
- 830 Huang, X., Ding, A., Gao, J., Zheng, B., Zhou, D., Qi, X., et al. (2021). Enhanced secondary
831 pollution offset reduction of primary emissions during COVID-19 lockdown in China.
832 *National Science Review*, *8*(2). <https://doi.org/10.1093/nsr/nwaa137>
- 833 Hudman, R. C., Moore, N. E., Mebust, A. K., Martin, R. V., Russell, A. R., Valin, L. C., &
834 Cohen, R. C. (2012). Steps towards a mechanistic model of global soil nitric oxide
835 emissions: implementation and space based-constraints. *Atmospheric Chemistry and*
836 *Physics*, *12*(16), 7779–7795. <https://doi.org/10.5194/acp-12-7779-2012>
- 837 Itahashi, S., Yumimoto, K., Uno, I., Hayami, H., Fujita, S., Pan, Y., & Wang, Y. (2018). A 15-
838 year record (2001–2015) of the ratio of nitrate to non-sea-salt sulfate in precipitation over
839 East Asia. *Atmospheric Chemistry and Physics*, *18*(4), 2835–2852.
840 <https://doi.org/10.5194/acp-18-2835-2018>
- 841 Jaeglé, L., Shah, V., Thornton, J. A., Lopez-Hilfiker, F. D., Lee, B. H., McDuffie, E. E., et al.
842 (2018). Nitrogen Oxides Emissions, Chemistry, Deposition, and Export Over the Northeast
843 United States During the WINTER Aircraft Campaign. *Journal of Geophysical Research:*
844 *Atmospheres*, *123*(21), 12,368–12,393. <https://doi.org/10.1029/2018JD029133>
- 845 Kalberer, M., Ammann, M., Arens, F., Gäggeler, H. W., & Baltensperger, U. (1999).
846 Heterogeneous formation of nitrous acid (HONO) on soot aerosol particles. *Journal of*
847 *Geophysical Research: Atmospheres*, *104*(D11), 13825–13832.
848 <https://doi.org/10.1029/1999JD900141>
- 849 Kasibhatla, P., Sherwen, T., Evans, M. J., Carpenter, L. J., Reed, C., Alexander, B., et al. (2018).
850 Global impact of nitrate photolysis in sea-salt aerosol on NO_x, OH, and O₃ in the marine
851 boundary layer. *Atmospheric Chemistry and Physics*, *18*(15), 11185–11203.
852 <https://doi.org/10.5194/acp-18-11185-2018>
- 853 Kenagy, H. S., Sparks, T. L., Ebben, C. J., Wooldrige, P. J., Lopez-Hilfiker, F. D., Lee, B. H., et
854 al. (2018). NO_x Lifetime and NO_y Partitioning During WINTER. *Journal of Geophysical*
855 *Research: Atmospheres*, *123*(17), 9813–9827. <https://doi.org/10.1029/2018JD028736>
- 856 Kleffmann, J., Becker, K. H., Lackhoff, M., & Wiesen, P. (1999). Heterogeneous conversion of
857 NO₂ on carbonaceous surfaces. *Physical Chemistry Chemical Physics*, *1*(24), 5443–5450.
858 <https://doi.org/10.1039/a905545b>
- 859 Lamsal, L. N., Martin, R. V., van Donkelaar, A., Steinbacher, M., Celarier, E. A., Bucsela, E., et
860 al. (2008). Ground-level nitrogen dioxide concentrations inferred from the satellite-borne
861 Ozone Monitoring Instrument. *Journal of Geophysical Research*, *113*(D16), D16308.
862 <https://doi.org/10.1029/2007JD009235>
- 863 Le, T., Wang, Y., Liu, L., Yang, J., Yung, Y. L., Li, G., & Seinfeld, J. H. (2020). Unexpected air
864 pollution with marked emission reductions during the COVID-19 outbreak in China.

- 865 *Science*, 369(6504), 702–706. <https://doi.org/10.1126/science.abb7431>
- 866 Lelieveld, J., Evans, J. S., Fnais, M., Giannadaki, D., & Pozzer, A. (2015). The contribution of
867 outdoor air pollution sources to premature mortality on a global scale. *Nature*, 525(7569),
868 367–371. <https://doi.org/10.1038/nature15371>
- 869 Leung, D. M., Shi, H., Zhao, B., Wang, J., Ding, E. M., Gu, Y., et al. (2020). Wintertime
870 Particulate Matter Decrease Buffered by Unfavorable Chemical Processes Despite
871 Emissions Reductions in China. *Geophysical Research Letters*, 47(14).
872 <https://doi.org/10.1029/2020GL087721>
- 873 Li, H., Cheng, J., Zhang, Q., Zheng, B., Zhang, Y., Zheng, G., & He, K. (2019). Rapid transition
874 in winter aerosol composition in Beijing from 2014 to 2017: response to clean air actions.
875 *Atmospheric Chemistry and Physics*, 19(17), 11485–11499. [https://doi.org/10.5194/acp-19-](https://doi.org/10.5194/acp-19-11485-2019)
876 11485-2019
- 877 Li, J., Chen, X., Wang, Z., Du, H., Yang, W., Sun, Y., et al. (2018). Radiative and heterogeneous
878 chemical effects of aerosols on ozone and inorganic aerosols over East Asia. *Science of the*
879 *Total Environment*, 622–623, 1327–1342. <https://doi.org/10.1016/j.scitotenv.2017.12.041>
- 880 Li, K., Jacob, D. J., Liao, H., Zhu, J., Shah, V., Shen, L., et al. (2019). A two-pollutant strategy
881 for improving ozone and particulate air quality in China. *Nature Geoscience*, 12(11), 906–
882 910. <https://doi.org/10.1038/s41561-019-0464-x>
- 883 Li, K., Jacob, D. J., Liao, H., Shen, L., Zhang, Q., & Bates, K. H. (2019). Anthropogenic drivers
884 of 2013–2017 trends in summer surface ozone in China. *Proceedings of the National*
885 *Academy of Sciences of the United States of America*, 116(2), 422–427.
886 <https://doi.org/10.1073/pnas.1812168116>
- 887 Li, L., Hoffmann, M. R., & Colussi, A. J. (2018). Role of Nitrogen Dioxide in the Production of
888 Sulfate during Chinese Haze-Aerosol Episodes. *Environmental Science & Technology*,
889 52(5), 2686–2693. <https://doi.org/10.1021/acs.est.7b05222>
- 890 Li, M., Zhang, Q., Kurokawa, J., Woo, J.-H., He, K., Lu, Z., et al. (2017). MIX: a mosaic Asian
891 anthropogenic emission inventory under the international collaboration framework of the
892 MICS-Asia and HTAP. *Atmospheric Chemistry and Physics*, 17(2), 935–963.
893 <https://doi.org/10.5194/acp-17-935-2017>
- 894 Lin, J. T., & McElroy, M. B. (2010). Impacts of boundary layer mixing on pollutant vertical
895 profiles in the lower troposphere: Implications to satellite remote sensing. *Atmospheric*
896 *Environment*, 44(14), 1726–1739. <https://doi.org/10.1016/j.atmosenv.2010.02.009>
- 897 Liu, C., Ma, Z., Mu, Y., Liu, J., Zhang, C., Zhang, Y., et al. (2017). The levels, variation
898 characteristics, and sources of atmospheric non-methane hydrocarbon compounds during
899 wintertime in Beijing, China. *Atmospheric Chemistry and Physics*, 17(17), 10633–10649.
900 <https://doi.org/10.5194/acp-17-10633-2017>
- 901 Liu, H., Jacob, D. J., Bey, I., & Yantosca, R. M. (2001). Constraints from ²¹⁰Pb and ⁷Be on
902 wet deposition and transport in a global three-dimensional chemical tracer model driven by
903 assimilated meteorological fields. *Journal of Geophysical Research: Atmospheres*,
904 106(D11), 12109–12128. <https://doi.org/10.1029/2000JD900839>
- 905 Liu, P., Ye, C., Xue, C., Zhang, C., Mu, Y., & Sun, X. (2020). Formation mechanisms of

- 906 atmospheric nitrate and sulfate during the winter haze pollution periods in Beijing: gas-
907 phase, heterogeneous and aqueous-phase chemistry. *Atmospheric Chemistry and Physics*,
908 20(7), 4153–4165. <https://doi.org/10.5194/acp-20-4153-2020>
- 909 Liu, Y., Lu, K., Li, X., Dong, H., Tan, Z., Wang, H., et al. (2019). A Comprehensive Model Test
910 of the HONO Sources Constrained to Field Measurements at Rural North China Plain.
911 *Environmental Science & Technology*, 53(7), 3517–3525.
912 <https://doi.org/10.1021/acs.est.8b06367>
- 913 Lu, K., Fuchs, H., Hofzumahaus, A., Tan, Z., Wang, H., Zhang, L., et al. (2019). Fast
914 Photochemistry in Wintertime Haze: Consequences for Pollution Mitigation Strategies.
915 *Environmental Science & Technology*, 53(18), 10676–10684.
916 <https://doi.org/10.1021/acs.est.9b02422>
- 917 Mao, J., Fan, S., Jacob, D. J., & Travis, K. R. (2013). Radical loss in the atmosphere from Cu-Fe
918 redox coupling in aerosols. *Atmospheric Chemistry and Physics*, 13(2), 509–519.
919 <https://doi.org/10.5194/acp-13-509-2013>
- 920 Marais, E. A., & Wiedinmyer, C. (2016). Air Quality Impact of Diffuse and Inefficient
921 Combustion Emissions in Africa (DICE-Africa). *Environmental Science & Technology*,
922 50(19), 10739–10745. <https://doi.org/10.1021/acs.est.6b02602>
- 923 McDonald, B. C., De Gouw, J. A., Gilman, J. B., Jathar, S. H., Akherati, A., Cappa, C. D., et al.
924 (2018). Volatile chemical products emerging as largest petrochemical source of urban
925 organic emissions. *Science*, 359(6377), 760–764. <https://doi.org/10.1126/science.aag0524>
- 926 McDuffie, E. E., Fibiger, D. L., Dubé, W. P., Lopez-Hilfiker, F., Lee, B. H., Thornton, J. A., et
927 al. (2018). Heterogeneous N₂O₅ Uptake During Winter: Aircraft Measurements During the
928 2015 WINTER Campaign and Critical Evaluation of Current Parameterizations. *Journal of*
929 *Geophysical Research: Atmospheres*, 123(8), 4345–4372.
930 <https://doi.org/10.1002/2018JD028336>
- 931 Michalski, G., Scott, Z., Kabling, M., & Thiemens, M. H. (2003). First measurements and
932 modeling of $\Delta 17\text{O}$ in atmospheric nitrate. *Geophysical Research Letters*, 30(16).
933 <https://doi.org/10.1029/2003GL017015>
- 934 Morin, S., Sander, R., & Savarino, J. (2011). Simulation of the diurnal variations of the oxygen
935 isotope anomaly ($\Delta 17\text{O}$) of reactive atmospheric species. *Atmospheric Chemistry and*
936 *Physics*, 11(8), 3653–3671. <https://doi.org/10.5194/acp-11-3653-2011>
- 937 Murray, L. T., Jacob, D. J., Logan, J. A., Hudman, R. C., & Koshak, W. J. (2012). Optimized
938 regional and interannual variability of lightning in a global chemical transport model
939 constrained by LIS/OTD satellite data. *Journal of Geophysical Research: Atmospheres*,
940 117(D20). <https://doi.org/10.1029/2012JD017934>
- 941 Neu, J. L., Prather, M. J., & Penner, J. E. (2007). Global atmospheric chemistry: Integrating over
942 fractional cloud cover. *Journal of Geophysical Research*, 112(D11), D11306.
943 <https://doi.org/10.1029/2006JD008007>
- 944 Reed, C., Evans, M. J., Di Carlo, P., Lee, J. D., & Carpenter, L. J. (2016). Interferences in
945 photolytic NO₂ measurements: explanation for
946 an apparent missing oxidant? *Atmospheric Chemistry and Physics*, 16(7), 4707–4724.
947 <https://doi.org/10.5194/acp-16-4707-2016>

- 948 Savarino, J., Morin, S., Erbland, J., Grannec, F., Patey, M. D., Vicars, W., et al. (2013). Isotopic
949 composition of atmospheric nitrate in a tropical marine boundary layer. *Proceedings of the*
950 *National Academy of Sciences*, *110*(44), 17668–17673.
951 <https://doi.org/10.1073/pnas.1216639110>
- 952 Shah, V., Jaeglé, L., Thornton, J. A., Lopez-Hilfiker, F. D., Lee, B. H., Schroder, J. C., et al.
953 (2018). Chemical feedbacks weaken the wintertime response of particulate sulfate and
954 nitrate to emissions reductions over the eastern United States. *Proceedings of the National*
955 *Academy of Sciences of the United States of America*, *115*(32), 8110–8115.
956 <https://doi.org/10.1073/pnas.1803295115>
- 957 Shah, V., Jacob, D. J., Li, K., Silvern, R. F., Zhai, S., Liu, M., et al. (2020). Effect of changing
958 NO_x lifetime on the seasonality and long-term trends of satellite-observed tropospheric
959 NO₂ columns over China. *Atmospheric Chemistry and Physics*, *20*(3), 1483–1495.
960 <https://doi.org/10.5194/acp-20-1483-2020>
- 961 Shao, J., Chen, Q., Wang, Y., Lu, X., He, P., Sun, Y., et al. (2019). Heterogeneous sulfate
962 aerosol formation mechanisms during wintertime Chinese haze events: air quality model
963 assessment using observations of sulfate oxygen isotopes in Beijing. *Atmospheric*
964 *Chemistry and Physics*, *19*(9), 6107–6123. <https://doi.org/10.5194/acp-19-6107-2019>
- 965 Sheng, J., Zhao, D., Ding, D., Li, X., Huang, M., Gao, Y., et al. (2018). Characterizing the level,
966 photochemical reactivity, emission, and source contribution of the volatile organic
967 compounds based on PTR-TOF-MS during winter haze period in Beijing, China.
968 *Atmospheric Research*, *212*, 54–63. <https://doi.org/10.1016/j.atmosres.2018.05.005>
- 969 Sherwen, T., Evans, M. J., Sommariva, R., Hollis, L. D. J., Ball, S. M., Monks, P. S., et al.
970 (2017). Effects of halogens on European air-quality. *Faraday Discussions*, *200*, 75–100.
971 <https://doi.org/10.1039/C7FD00026J>
- 972 Shi, G., Xu, J., Shi, X., Liu, B., Bi, X., Xiao, Z., et al. (2019). Aerosol pH Dynamics During
973 Haze Periods in an Urban Environment in China: Use of Detailed, Hourly, Speciated
974 Observations to Study the Role of Ammonia Availability and Secondary Aerosol Formation
975 and Urban Environment. *Journal of Geophysical Research: Atmospheres*, *124*(16), 9730–
976 9742. <https://doi.org/10.1029/2018JD029976>
- 977 Song, C., He, J., Wu, L., Jin, T., Chen, X., Li, R., et al. (2017). Health burden attributable to
978 ambient PM_{2.5} in China. *Environmental Pollution*, *223*, 575–586.
979 <https://doi.org/10.1016/J.ENVPOL.2017.01.060>
- 980 Song, W., Liu, X.-Y., Wang, Y.-L., Tong, Y.-D., Bai, Z.-P., & Liu, C.-Q. (2020). Nitrogen
981 isotope differences between atmospheric nitrate and corresponding nitrogen oxides: A new
982 constraint using oxygen isotopes. *Science of The Total Environment*, *701*, 134515.
983 <https://doi.org/10.1016/j.scitotenv.2019.134515>
- 984 Sun, J., Wang, Y., Wu, F., Tang, G., Wang, L., Wang, Y., & Yang, Y. (2018). Vertical
985 characteristics of VOCs in the lower troposphere over the North China Plain during
986 pollution periods. *Environmental Pollution*, *236*, 907–915.
987 <https://doi.org/10.1016/j.envpol.2017.10.051>
- 988 Sun, Y., Lei, L., Zhou, W., Chen, C., He, Y., Sun, J., et al. (2020). A chemical cocktail during
989 the COVID-19 outbreak in Beijing, China: Insights from six-year aerosol particle

- 990 composition measurements during the Chinese New Year holiday. *Science of the Total*
991 *Environment*, 742, 140739. <https://doi.org/10.1016/j.scitotenv.2020.140739>
- 992 Tan, F., Tong, S., Jing, B., Hou, S., Liu, Q., Li, K., et al. (2016). Heterogeneous reactions of NO
993 2 with CaCO₃–(NH₄)₂SO₄ mixtures at different relative humidities. *Atmospheric*
994 *Chemistry and Physics*, 16(13), 8081–8093. <https://doi.org/10.5194/acp-16-8081-2016>
- 995 Tan, F., Jing, B., Tong, S., & Ge, M. (2017). The effects of coexisting Na₂SO₄ on heterogeneous
996 uptake of NO₂ on CaCO₃ particles at various RHs. *Science of the Total Environment*, 586,
997 930–938. <https://doi.org/10.1016/j.scitotenv.2017.02.072>
- 998 Tan, Z., Lu, K., Jiang, M., Su, R., Wang, H., Lou, S., et al. (2019). Daytime atmospheric
999 oxidation capacity in four Chinese megacities during the photochemically polluted season: a
1000 case study based on box model simulation. *Atmospheric Chemistry and Physics*, 19(6),
1001 3493–3513. <https://doi.org/10.5194/acp-19-3493-2019>
- 1002 Tham, Y. J., Wang, Z., Li, Q., Yun, H., Wang, W., Wang, X., et al. (2016). Significant
1003 concentrations of nitryl chloride sustained in the morning: investigations of the causes and
1004 impacts on ozone production in a polluted region of northern China. *Atmospheric Chemistry*
1005 *and Physics*, 16(23), 14959–14977. <https://doi.org/10.5194/acp-16-14959-2016>
- 1006 Thornton, J., & Abbatt, J. P. D. (2005). Measurements of HO₂ uptake to aqueous aerosol: Mass
1007 accommodation coefficients and net reactive loss. *Journal of Geophysical Research*,
1008 110(D8), D08309. <https://doi.org/10.1029/2004JD005402>
- 1009 Vicars, W. C., & Savarino, J. (2014). Quantitative constraints on the 17O-excess ($\Delta 17O$)
1010 signature of surface ozone: Ambient measurements from 50°N to 50°S using the nitrite-
1011 coated filter technique. *Geochimica et Cosmochimica Acta*, 135, 270–287.
1012 <https://doi.org/10.1016/j.gca.2014.03.023>
- 1013 Wang, Jiaqi, Zhang, X., Guo, J., Wang, Z., & Zhang, M. (2017). Observation of nitrous acid
1014 (HONO) in Beijing, China: Seasonal variation, nocturnal formation and daytime budget.
1015 *Science of The Total Environment*, 587–588, 350–359.
1016 <https://doi.org/10.1016/j.scitotenv.2017.02.159>
- 1017 Wang, Junfeng, Li, J., Ye, J., Zhao, J., Wu, Y., Hu, J., et al. (2020). Fast sulfate formation from
1018 oxidation of SO₂ by NO₂ and HONO observed in Beijing haze. *Nature Communications*,
1019 11(1), 2844. <https://doi.org/10.1038/s41467-020-16683-x>
- 1020 Wang, W., Li, X., Shao, M., Hu, M., Zeng, L., Wu, Y., & Tan, T. (2019). The impact of aerosols
1021 on photolysis frequencies and ozone production in Beijing during the 4-year period 2012–
1022 2015. *Atmospheric Chemistry and Physics*, 19(14), 9413–9429. [https://doi.org/10.5194/acp-](https://doi.org/10.5194/acp-19-9413-2019)
1023 19-9413-2019
- 1024 Wang, X., Jacob, D. J., Eastham, S. D., Sulprizio, M. P., Zhu, L., Chen, Q., et al. (2019). The
1025 role of chlorine in global tropospheric chemistry. *Atmospheric Chemistry and Physics*,
1026 19(6), 3981–4003. <https://doi.org/10.5194/acp-19-3981-2019>
- 1027 Wang, X., Jacob, D. J., Fu, X., Wang, T., Le Breton, M., Hallquist, M., et al. (2020). Effects of
1028 anthropogenic chlorine on PM_{2.5} and ozone air quality in China. *Environmental Science &*
1029 *Technology*, acs.est.0c02296. <https://doi.org/10.1021/acs.est.0c02296>
- 1030 Wang, Yan-Li, Song, W., Yang, W., Sun, X., Tong, Y., Wang, X., et al. (2019). Influences of

- 1031 Atmospheric Pollution on the Contributions of Major Oxidation Pathways to PM 2.5 Nitrate
1032 Formation in Beijing. *Journal of Geophysical Research: Atmospheres*, 124(7), 4174–4185.
1033 <https://doi.org/10.1029/2019JD030284>
- 1034 Wang, Yuhang, Jacob, D. J., & Logan, J. A. (1998). Global simulation of tropospheric O₃-NO_x-
1035 hydrocarbon chemistry: 1. Model formulation. *Journal of Geophysical Research:*
1036 *Atmospheres*, 103(D9), 10713–10725. <https://doi.org/10.1029/98JD00158>
- 1037 van der Werf, G. R., Randerson, J. T., Giglio, L., van Leeuwen, T. T., Chen, Y., Rogers, B. M.,
1038 et al. (2017). Global fire emissions estimates during 1997–2016. *Earth System Science*
1039 *Data*, 9(2), 697–720. <https://doi.org/10.5194/essd-9-697-2017>
- 1040 Womack, C. C., McDuffie, E. E., Edwards, P. M., Bares, R., Gouw, J. A., Docherty, K. S., et al.
1041 (2019). An Odd Oxygen Framework for Wintertime Ammonium Nitrate Aerosol Pollution
1042 in Urban Areas: NO_x and VOC Control as Mitigation Strategies. *Geophysical Research*
1043 *Letters*, 46(9), 4971–4979. <https://doi.org/10.1029/2019GL082028>
- 1044 Xia, M., Wang, W., Wang, Z., Gao, J., Li, H., Liang, Y., et al. (2019). Heterogeneous uptake of
1045 N₂O₅ in sand dust and urban aerosols observed during the dry season in Beijing.
1046 *Atmosphere*, 10(4), 204. <https://doi.org/10.3390/ATMOS10040204>
- 1047 Xu, Q., Wang, S., Jiang, J., Bhattarai, N., Li, X., Chang, X., et al. (2019). Nitrate dominates the
1048 chemical composition of PM_{2.5} during haze event in Beijing, China. *Science of the Total*
1049 *Environment*, 689, 1293–1303. <https://doi.org/10.1016/j.scitotenv.2019.06.294>
- 1050 Yan, Y., Peng, L., Li, R., Li, Y., Li, L., & Bai, H. (2017). Concentration, ozone formation
1051 potential and source analysis of volatile organic compounds (VOCs) in a thermal power
1052 station centralized area: A study in Shuozhou, China. *Environmental Pollution*, 223, 295–
1053 304. <https://doi.org/10.1016/j.envpol.2017.01.026>
- 1054 Ye, C., Zhang, N., Gao, H., & Zhou, X. (2017). Photolysis of Particulate Nitrate as a Source of
1055 HONO and NO_x. *Environmental Science & Technology*, 51(12), 6849–6856.
1056 <https://doi.org/10.1021/acs.est.7b00387>
- 1057 Yu, C., Wang, Z., Xia, M., Fu, X., Wang, W., Tham, Y. J., et al. (2020). Heterogeneous N₂O₅
1058 reactions on atmospheric aerosols at four Chinese sites: improving model representation of
1059 uptake parameters. *Atmospheric Chemistry and Physics*, 20(7), 4367–4378.
1060 <https://doi.org/10.5194/acp-20-4367-2020>
- 1061 Yu, D., Tan, Z., Lu, K., Ma, X., Li, X., Chen, S., et al. (2020). An explicit study of local ozone
1062 budget and NO_x-VOCs sensitivity in Shenzhen China. *Atmospheric Environment*, 224,
1063 117304. <https://doi.org/10.1016/j.atmosenv.2020.117304>
- 1064 Zhang, B., Zhao, B., Zuo, P., Huang, Z., & Zhang, J. (2017). Ambient peroxyacyl nitrate
1065 concentration and regional transportation in Beijing. *Atmospheric Environment*, 166, 543–
1066 550. <https://doi.org/10.1016/j.atmosenv.2017.07.053>
- 1067 Zhang, G., Xia, L., Zang, K., Xu, W., Zhang, F., Liang, L., et al. (2020). The abundance and
1068 inter-relationship of atmospheric peroxyacetyl nitrate (PAN), peroxypropionyl nitrate
1069 (PPN), O₃, and NO_y during the wintertime in Beijing, China. *Science of the Total*
1070 *Environment*, 718, 137388. <https://doi.org/10.1016/j.scitotenv.2020.137388>
- 1071 Zhang, H., Xu, X., Lin, W., & Wang, Y. (2014). Wintertime peroxyacetyl nitrate (PAN) in the

- 1072 megacity Beijing: Role of photochemical and meteorological processes. *Journal of*
1073 *Environmental Sciences (China)*, 26(1), 83–96. <https://doi.org/10.1016/S1001->
1074 0742(13)60384-8
- 1075 Zhang, J., An, J., Qu, Y., Liu, X., & Chen, Y. (2019). Impacts of potential HONO sources on the
1076 concentrations of oxidants and secondary organic aerosols in the Beijing-Tianjin-Hebei
1077 region of China. *Science of The Total Environment*, 647, 836–852.
1078 <https://doi.org/10.1016/j.scitotenv.2018.08.030>
- 1079 Zhang, L., Gong, S., Padro, J., & Barrie, L. (2001). A size-segregated particle dry deposition
1080 scheme for an atmospheric aerosol module. *Atmospheric Environment*, 35(3), 549–560.
1081 [https://doi.org/10.1016/S1352-2310\(00\)00326-5](https://doi.org/10.1016/S1352-2310(00)00326-5)
- 1082 Zhang, Y.-L., & Cao, F. (2015). Fine particulate matter (PM_{2.5}) in China at a city level.
1083 *Scientific Reports*, 5(1), 14884. <https://doi.org/10.1038/srep14884>
- 1084 Zheng, B., Tong, D., Li, M., Liu, F., Hong, C., Geng, G., et al. (2018). Trends in China's
1085 anthropogenic emissions since 2010 as the consequence of clean air actions. *Atmospheric*
1086 *Chemistry and Physics*, 18(19), 14095–14111. <https://doi.org/10.5194/acp-18-14095-2018>
- 1087 Zhou, W., Zhao, J., Ouyang, B., Mehra, A., Xu, W., Wang, Y., et al. (2018). Production of N₂O₅
1088 and ClNO₂ in summer in urban Beijing, China. *Atmospheric Chemistry and Physics*,
1089 18(16), 11581–11597. <https://doi.org/10.5194/acp-18-11581-2018>
- 1090 Zhou, W., Gao, M., He, Y., Wang, Q., Xie, C., Xu, W., et al. (2019). Response of aerosol
1091 chemistry to clean air action in Beijing, China: Insights from two-year ACSM
1092 measurements and model simulations. *Environmental Pollution*, 255, 113345.
1093 <https://doi.org/10.1016/j.envpol.2019.113345>
1094

1095 **Other supporting references**

- 1096 Acton, W. J. F., Huang, Z., Davison, B., Drysdale, W. S., Fu, P., Hollaway, M., et al. (2020).
1097 Surface–atmosphere fluxes of volatile organic compounds in Beijing. *Atmospheric*
1098 *Chemistry and Physics*, 20(23), 15101–15125. <https://doi.org/10.5194/acp-20-15101-2020>
- 1099 Fu, X., Wang, T., Zhang, L., Li, Q., Wang, Z., Xia, M., et al. (2019). The significant contribution
1100 of HONO to secondary pollutants during a severe winter pollution event in southern China.
1101 *Atmospheric Chemistry and Physics*, 19(1), 1–14. <https://doi.org/10.5194/acp-19-1-2019>
- 1102 Haskins, J. D., Lopez-Hilfiker, F. D., Lee, B. H., Shah, V., Wolfe, G. M., DiGangi, J., et al.
1103 (2019). Anthropogenic Control Over Wintertime Oxidation of Atmospheric Pollutants.
1104 *Geophysical Research Letters*, 46(24), 14826–14835.
1105 <https://doi.org/10.1029/2019GL085498>
- 1106 Hoffmann, E. H., Tilgner, A., Vogelsberg, U., Wolke, R., & Herrmann, H. (2019). Near-Explicit
1107 Multiphase Modeling of Halogen Chemistry in a Mixed Urban and Maritime Coastal Area.
1108 *ACS Earth and Space Chemistry*, 3(11), 2452–2471.
1109 <https://doi.org/10.1021/acsearthspacechem.9b00184>
- 1110 Li, D., Xue, L., Wen, L., Wang, X., Chen, T., Mellouki, A., et al. (2018). Characteristics and
1111 sources of nitrous acid in an urban atmosphere of northern China: Results from 1-yr
1112 continuous observations. *Atmospheric Environment*, 182, 296–306.
1113 <https://doi.org/10.1016/J.ATMOSENV.2018.03.033>
- 1114 Li, J., Xie, S. D., Zeng, L. M., Li, L. Y., Li, Y. Q., & Wu, R. R. (2015). Characterization of
1115 ambient volatile organic compounds and their sources in Beijing, before, during, and after
1116 Asia-Pacific Economic Cooperation China 2014. *Atmospheric Chemistry and Physics*,
1117 15(14), 7945–7959. <https://doi.org/10.5194/acp-15-7945-2015>
- 1118 Li, K., Li, J., Tong, S., Wang, W., Huang, R.-J., & Ge, M. (2019). Characteristics of wintertime
1119 VOCs in suburban and urban Beijing: concentrations, emission ratios, and festival effects.
1120 *Atmospheric Chemistry and Physics*, 19(12), 8021–8036. [https://doi.org/10.5194/acp-19-](https://doi.org/10.5194/acp-19-8021-2019)
1121 [8021-2019](https://doi.org/10.5194/acp-19-8021-2019)
- 1122 Li, Q., Badia, A., Wang, T., Sarwar, G., Fu, X., Zhang, L., et al. (2020). Potential Effect of
1123 Halogens on Atmospheric Oxidation and Air Quality in China. *Journal of Geophysical*
1124 *Research: Atmospheres*, 125(9). <https://doi.org/10.1029/2019JD032058>
- 1125 McCulloch, A., Aucott, M. L., Benkovitz, C. M., Graedel, T. E., Kleiman, G., Midgley, P. M., &
1126 Li, Y.-F. (1999). Global emissions of hydrogen chloride and chloromethane from coal
1127 combustion, incineration and industrial activities: Reactive Chlorine Emissions Inventory.
1128 *Journal of Geophysical Research: Atmospheres*, 104(D7), 8391–8403.
1129 <https://doi.org/10.1029/1999JD900025>
- 1130 Romer, P. S., Wooldridge, P. J., Crouse, J. D., Kim, M. J., Wennberg, P. O., Dibb, J. E., et al.
1131 (2018). Constraints on Aerosol Nitrate Photolysis as a Potential Source of HONO and NO
1132 x. *Environmental Science & Technology*, 52(23), 13738–13746.
1133 <https://doi.org/10.1021/acs.est.8b03861>
- 1134 Shi, Y., Hu, F., Xiao, Z., Fan, G., & Zhang, Z. (2020). Comparison of four different types of
1135 planetary boundary layer heights during a haze episode in Beijing. *Science of the Total*
1136 *Environment*, 711, 134928. <https://doi.org/10.1016/j.scitotenv.2019.134928>

- 1137 Su, T., Li, Z., & Kahn, R. (2018). Relationships between the planetary boundary layer height and
1138 surface pollutants derived from lidar observations over China: regional pattern and
1139 influencing factors. *Atmospheric Chemistry and Physics*, *18*(21), 15921–15935.
1140 <https://doi.org/10.5194/acp-18-15921-2018>
- 1141 Tang, G., Zhang, J., Zhu, X., Song, T., Münkel, C., Hu, B., et al. (2016). Mixing layer height and
1142 its implications for air pollution over Beijing, China. *Atmospheric Chemistry and Physics*,
1143 *16*(4), 2459–2475. <https://doi.org/10.5194/acp-16-2459-2016>
- 1144
- 1145
- 1146

1147 References From the Supporting Information

1148

- 1149 Acton, W. J. F., Huang, Z., Davison, B., Drysdale, W. S., Fu, P., Hollaway, M., et al. (2020).
1150 Surface–atmosphere fluxes of volatile organic compounds in Beijing. *Atmospheric*
1151 *Chemistry and Physics*, 20(23), 15101–15125. <https://doi.org/10.5194/acp-20-15101-2020>
- 1152 Fu, X., Wang, T., Zhang, L., Li, Q., Wang, Z., Xia, M., et al. (2019). The significant contribution
1153 of HONO to secondary pollutants during a severe winter pollution event in southern China.
1154 *Atmospheric Chemistry and Physics*, 19(1), 1–14. <https://doi.org/10.5194/acp-19-1-2019>
- 1155 Haskins, J. D., Lopez-Hilfiker, F. D., Lee, B. H., Shah, V., Wolfe, G. M., DiGangi, J., et al.
1156 (2019). Anthropogenic Control Over Wintertime Oxidation of Atmospheric Pollutants.
1157 *Geophysical Research Letters*, 46(24), 14826–14835.
1158 <https://doi.org/10.1029/2019GL085498>
- 1159 Hoffmann, E. H., Tilgner, A., Vogelsberg, U., Wolke, R., & Herrmann, H. (2019). Near-Explicit
1160 Multiphase Modeling of Halogen Chemistry in a Mixed Urban and Maritime Coastal Area.
1161 *ACS Earth and Space Chemistry*, 3(11), 2452–2471.
1162 <https://doi.org/10.1021/acsearthspacechem.9b00184>
- 1163 Li, D., Xue, L., Wen, L., Wang, X., Chen, T., Mellouki, A., et al. (2018). Characteristics and
1164 sources of nitrous acid in an urban atmosphere of northern China: Results from 1-yr
1165 continuous observations. *Atmospheric Environment*, 182, 296–306.
1166 <https://doi.org/10.1016/J.ATMOSENV.2018.03.033>
- 1167 Li, J., Xie, S. D., Zeng, L. M., Li, L. Y., Li, Y. Q., & Wu, R. R. (2015). Characterization of
1168 ambient volatile organic compounds and their sources in Beijing, before, during, and after
1169 Asia-Pacific Economic Cooperation China 2014. *Atmospheric Chemistry and Physics*,
1170 15(14), 7945–7959. <https://doi.org/10.5194/acp-15-7945-2015>
- 1171 Li, K., Li, J., Tong, S., Wang, W., Huang, R.-J., & Ge, M. (2019). Characteristics of wintertime
1172 VOCs in suburban and urban Beijing: concentrations, emission ratios, and festival effects.
1173 *Atmospheric Chemistry and Physics*, 19(12), 8021–8036. [https://doi.org/10.5194/acp-19-](https://doi.org/10.5194/acp-19-8021-2019)
1174 8021-2019
- 1175 Li, Q., Badia, A., Wang, T., Sarwar, G., Fu, X., Zhang, L., et al. (2020). Potential Effect of
1176 Halogens on Atmospheric Oxidation and Air Quality in China. *Journal of Geophysical*
1177 *Research: Atmospheres*, 125(9). <https://doi.org/10.1029/2019JD032058>
- 1178 McCulloch, A., Aucott, M. L., Benkovitz, C. M., Graedel, T. E., Kleiman, G., Midgley, P. M., &
1179 Li, Y.-F. (1999). Global emissions of hydrogen chloride and chloromethane from coal
1180 combustion, incineration and industrial activities: Reactive Chlorine Emissions Inventory.
1181 *Journal of Geophysical Research: Atmospheres*, 104(D7), 8391–8403.
1182 <https://doi.org/10.1029/1999JD900025>
- 1183 Romer, P. S., Wooldridge, P. J., Crouse, J. D., Kim, M. J., Wennberg, P. O., Dibb, J. E., et al.
1184 (2018). Constraints on Aerosol Nitrate Photolysis as a Potential Source of HONO and NO
1185 x. *Environmental Science & Technology*, 52(23), 13738–13746.
1186 <https://doi.org/10.1021/acs.est.8b03861>
- 1187 Shi, Y., Hu, F., Xiao, Z., Fan, G., & Zhang, Z. (2020). Comparison of four different types of
1188 planetary boundary layer heights during a haze episode in Beijing. *Science of the Total*

- 1189 *Environment*, 711, 134928. <https://doi.org/10.1016/j.scitotenv.2019.134928>
- 1190 Su, T., Li, Z., & Kahn, R. (2018). Relationships between the planetary boundary layer height and
1191 surface pollutants derived from lidar observations over China: regional pattern and
1192 influencing factors. *Atmospheric Chemistry and Physics*, 18(21), 15921–15935.
1193 <https://doi.org/10.5194/acp-18-15921-2018>
- 1194 Tang, G., Zhang, J., Zhu, X., Song, T., Münkler, C., Hu, B., et al. (2016). Mixing layer height and
1195 its implications for air pollution over Beijing, China. *Atmospheric Chemistry and Physics*,
1196 16(4), 2459–2475. <https://doi.org/10.5194/acp-16-2459-2016>
1197
1198